U.S. DEPARTMENT OF COMMERCE
National Technical Information Service

PB-256 420

Carbon Oxidation Catalyst Mechanism Study for Fuel Cells

Exxon Research & Engineering Co.

Prepared For
Industrial Environmental Research Lab.

March 1976

TECHNICAL REPORT DATA
(Please read Instructions on the reverse before completing)

1. REPORT NO.	2.	3. RECIPIENT'S ACCESSION NO.
EPA-600/2-76-057		

4. TITLE AND SUBTITLE	5. REPORT DATE
Carbon Oxidation Catalyst Mechanism Study for Fuel Cells	March 1976
	6. PERFORMING ORGANIZATION CODE
7. AUTHOR(S)	8. PERFORMING ORGANIZATION REPORT NO.
Yen-Chi Pan	GRU. 2DYBA. 75/715520
9. PERFORMING ORGANIZATION NAME AND ADDRESS	10. PROGRAM ELEMENT NO.
Exxon Research and Engineering Company Government Research Laboratory Linden, New Jersey 07036	1AB013; ROAP 21BKB-006
	11. CONTRACT/GRANT NO.
	68-02-1831
12. SPONSORING AGENCY NAME AND ADDRESS	13. TYPE OF REPORT AND PERIOD COVERED
EPA, Office of Research and Development Industrial Environmental Research Laboratory Research Triangle Park, NC 27711	Final; 10/74-6/75
	14. SPONSORING AGENCY CODE
	EPA-ORD

15. SUPPLEMENTARY NOTES Project officer S. J. Bunas is no longer with EPA; for details, contact G. L. Johnson, Mail Drop 64, Ext 2815.

16. ABSTRACT The report gives results of a systematic examination of the polarization curves of oxygen reduction reaction on graphite, using a rotating disk-ring electrode. The reaction was studied in various electrolytes over a pH range of 14.6-1 and a temperature range of 25-75 C. The activity of this reaction was found to increase with decreasing $H^{(+)}$ concentration and increasing temperature. A linear relationship was found between the half-wave potential and pH value, with a slope of 40 mV per decade. The plot of ring current ratio versus the square root of angular speed in KOH solution clearly indicated a reaction sequence of: $O_2 + 2H^{(+)}$ yields $2e + H_2O_2$ which yields $2e + 2OH^{(-)}$. No 4-electron reduction of oxygen on carbon occurred. The level of carbon oxidation was higher in more acidic medium.

17. KEY WORDS AND DOCUMENT ANALYSIS

a. DESCRIPTORS		b. IDENTIFIERS/OPEN ENDED TERMS	c. COSATI Field/Group
Air Pollution	Current Density	Air Pollution Control	13B
Fuel Cells	Diffusion	Oxygen Reduction	10B
Catalysis	Activation	Rotating Disk-Ring Electrode	07D
Electrostatics	Polarization		20C
Graphite	Cathode	Tafel Slope	08G
Electrodes		Residual Current	09A

18. DISTRIBUTION STATEMENT	19. SECURITY CLASS (This Report)	21. NO. OF PAGES
Unlimited	Unclassified	69
	20. SECURITY CLASS (This page) Unclassified	22. PRICE $4.50/2.25

EPA Form 2220-1 (9-73)

PRICES SUBJECT TO CHANGE

PB 256 420

REPRODUCED BY
NATIONAL TECHNICAL
INFORMATION SERVICE
U. S. DEPARTMENT OF COMMERCE
SPRINGFIELD, VA. 22161

EPA-600/2-76-057
March 1976

CARBON OXIDATION CATALYST
MECHANISM STUDY FOR FUEL CELLS

by

Yen-Chi Pan

Exxon Research and Engineering Company
Government Research Laboratory
Linden, New Jersey 07036

Contract No. 68-02-1831
ROAP No. 21BKB-006
Program Element No. 1AB013

EPA Project Officer: S. J. Bunas

Industrial Environmental Research Laboratory
Office of Energy, Minerals, and Industry
Research Triangle Park, NC 27711

Prepared for

U.S. ENVIRONMENTAL PROTECTION AGENCY
Office of Research and Development
Washington, DC 20460

TABLE OF CONTENTS

	PAGE
LIST OF TABLES	iv
LIST OF FIGURES	v
1. INTRODUCTION	1
2. SUMMARY OF THE RESULTS	2
3. CONCLUSION	13
4. GENERAL DISCUSSION	15
5. EXPERIMENTAL METHOD	19
6. RESULTS AND DISCUSSIONS	25
ABBREVIATIONS AND SYMBOLS	58
REFERENCES	60

List of Tables

	Page
Table 1 - Electrochemical Potentials Related to Oxygen Reduction in Various Solutions	20
Table 2 - Parameters Involved in the Determination of the Oxygen Reduction Reaction Activity in KOH Solutions	30
Table 3 - Limiting Current For $O_2 + H^+ \xrightarrow{2e} H_2O_2(HO_2^-)$, ($mA/cm^2$)	34
Table 4 - Parameters Involved in the Determination of the Oxygen Reduction Reaction Activity in Solutions Containing Carbonate and Bicarbonate Ions	41
Table 5 - Parameters Involved in the Determination of the Oxygen Reduction Reaction Activity in Buffer Solutions Containing Phosphate	49
Table 6 - Parameter Involved in the Determination of the Oxygen Reduction Reaction Activity in Potassium Acetate-Acetic Acid Buffers and Sulfuric Acid	50

List of Figures

	Page
Figure 1 - The First Wave of the Polarization Curves in 0.1M/0.1M Solutions at 25°C	4
Figure 2 - The First Wave of the Polarization Curves in 0.1M/0.1M Solution at 75°C	5
Figure 3 - The First Wave of the Polarization Curves in 1M/1M Solution at 25°C	6
Figure 4 - The First Wave of the Polarization Curves in 1M/1M Solution at 75°C	7
Figure 5 - Half Wave Potential vs pH Value at 25°C	8
Figure 6 - Half Wave Potential vs pH Value at 75°C	9
Figure 7 - Exchange Current Density vs pH Value at 25°C	10
Figure 8 - Exchange Current Density vs pH Value at 75°C	11
Figure 9 - End View of Rotating Ring-Disk Electrode	17
Figure 10 - The Flow Pattern of a Rotating Disk Showing Streamlines	18
Figure 11 - Circuit Diagram for Rotating Ring-Disk Electrochemical Measurements	21
Figure 12 - Rotating Ring-Disk Electrode Assembly	23
Figure 13 - Reduction of Oxygen on Graphite in 0.1 N KOH at 25°C	26
Figure 14 - Reduction of Oxygen on Graphite in 0.5N KOH at 75°C	27
Figure 15 - Dependence of i_d/i_r on $w^{-\frac{1}{2}}$ for Oxygen Reduction in 0.1N KOH at 25°C	32
Figure 16 - Dependence of Limiting Current on $w^{\frac{1}{2}}$ in KOH Solution at 25°C	35
Figure 17 - Dependence of Limiting Current on $w^{\frac{1}{2}}$ in KOH Solution at 50°C	36
Figure 18 - Dependence of Limiting Current on $w^{\frac{1}{2}}$ in KOH Solution at 75°C	37

List of Figures (Cont'd)

	Page
Figure 19 - Reduction of Oxygen on Graphite in 2N/1M KOH-K_2CO_3 at 50°C	39
Figure 20 - Reduction of Oxygen on Graphite in 0.5M/0.5M K_2CO_3-$KHCO_3$ at 25°C	40
Figure 21 - Dependence of Limiting Current on $w^{\frac{1}{2}}$ in Solutions Containing Carbonate and Bicarbonate at 25°C	42
Figure 22 - Dependence of Limiting Current on $w^{\frac{1}{2}}$ in Solutions Containing Carbonate and Bicarbonate at 75°C	43
Figure 23 - Reduction of Oxygen on Graphite in Pre-electrolized 0.5M/0.5M K_2CO_3-$KHCO_3$ at 25°C	45
Figure 24 - Reduction of Oxygen on Graphite in 1M/1M KH_2PO_4-K_2HpO_4 at 75°C	46
Figure 25 - Reduction of Oxygen on Graphite in 1M/1M KAcO-HAcO at 75°C	47
Figure 26 - Reduction of Oxygen and Hydrogen Peroxide on Graphite in 1M/1M KAc - HAc at 75°C	48
Figure 27 - Dependence of Limiting Current on $w^{\frac{1}{2}}$ in Solutions Containing Phosphate at 25°C	51
Figure 28 - Dependence of Limiting Current on $w^{\frac{1}{2}}$ in Solutions Containing Phosphate at 75°C	52
Figure 29 - Reduction of Oxygen on Graphite in 1M/1M H_3PO_4-KH_2PO_4 at 75°C	55
Figure 30 - Reduction of Oxygen on Graphite in 0.1 N Sulfuric Acid at 75°C	56
Figure 31 - Dependence of Limiting Current on $w^{\frac{1}{2}}$ in Potassium Acetate-Acetic Acid Buffer and 0.1N Sulfuric Acid	57

1. INTRODUCTION

The objectives of this study were to develop information about the electrocatalytic behavior of carbon and the reaction kinetics of oxygen reduction, and to determine whether any combination of conditions, (temperature, electrolyte concentration, and pH value) exist in which a carbon cathode could operate sufficiently well to be used in a practical fuel cell. A systematic examination of the electrocatalytic activity for oxygen reduction in various electrolytes was conducted, using a rotating ring-disk electrode.

The oxygen or air cathode is undoubtedly the most desirable cathode for a variety of types of fuel cells, simply because of its relatively high open-circuit potential and the convenience of using air. However, there are difficulties involved in the widespread application of the air cathode. One of the major obstacles to its use is the cost and the scarcity of the best catalysts--the noble metals in group VIII, Pt, Pd, Os and Ir. Large quantities of these metals would be required for fuel cell applications and there simply are not enough of them; and the demand for this sort of use would drive the cost up higher than the present level. Therefore, an inexpensive and abundant material such as carbon is preferable for use as a cathode material.

Certain carbons are of considerable technical importance as substrates for the reduction of oxygen in alkaline electrolyte metal-air batteries and fuel cells (1). In some applications, they also have the advantage of selectivity; that is they are virtually inert in the oxidation of some soluble fuels. In fuel cells using either organic fuels or reformed CO_2--containing fuels, an electrolyte other than alkali may be required to prevent carbonate and bicarbonate formation. However, among the sparse literature concerning oxygen reduction on carbons, the emphasis is on pyrolytic graphite, and the measurements are limited to alkaline solutions at room temperature (2-5). Because of its untypically high crystalline order, pyrolytic graphite was not considered the appropriate carbon for this study. Therefore, a more representative carbon, commercial polycrystalline graphite, was chosen.

There have been numerous investigations of the cathodic oxygen reduction reaction, and it is generally agreed that hydrogen peroxide is the intermediate product. The reactions which may occur in the oxygen reduction reaction are listed below:

$$O_2 + 2H_2O + 4e \xrightarrow{K_1} 4OH^- \qquad (1a)$$

$$O_2 + 2H^+ + 2e \underset{K_{-2}}{\overset{K_2}{\rightleftharpoons}} H_2O_2{}^a \text{ (or } HO_2^-) \qquad (1b)$$

$$H_2O_2{}^a \text{ (or } HO_2^-) + 2e \xrightarrow{K_3} 2OH^- \qquad (1c)$$

$$2H_2O_2 \xrightarrow{K_4} O_2 + 2H_2O \qquad (1d)$$

$$H_2O_2{}^a \underset{K_6}{\overset{K_5}{\rightleftharpoons}} H_2O_2{}^b \qquad (1e)$$

Here $H_2O_2{}^a$ and $H_2O_2{}^b$ designate the adsorbed and desorbed H_2O_2 respectively.

A general scheme of the overall reaction, disregarding the material balance, can be expressed as

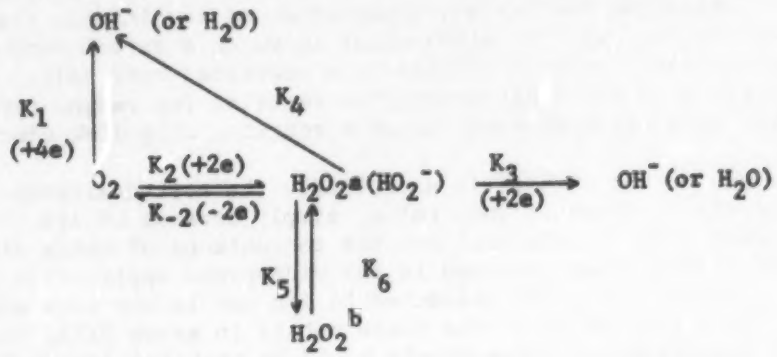

(1)

The rate constant K_i, which in general depends on the electrode potential, pertains to the ith reaction indicated in the scheme, e.g. K_4 represents the catalytic decomposition of $H_2O_2(HO_2^-)$ yielding O_2 and OH^-. The performance of the electrode depends to a large extent on the pathway of the reaction and its reaction rate.

In this study, a rotating ring-disk electrode technique was used to study the oxygen reduction mechanism. This technique is the most informative method of investigating the complex series of reactions involved in the oxygen reduction. In the ring-disk electrode, the concentric ring which is very slightly separated from the disk, can be set at a suitable potential to monitor quantitatively the H_2O_2 (or HO_2^-) production from the disk. The plots of the disk to ring current ratio, id/ir, obtained at constant potential versus $\omega^{\frac{1}{2}}$ (ω-angular velocity of the rotating electrode) can serve as diagnostic criteria in distinguishing the pathways of reduction, as well as means to obtain rate constant of various processes involved. A rotating graphite disk with a gold ring electrode has been used for this study.

2. SUMMARY OF THE RESULTS

The polarization curves of oxygen reduction reaction on graphite were systematically examined by using a rotating disk-ring electrode. The reaction was studied in various electrolytes, over a pH range from 14.6 to 1 and a temperature range from 25°C to 75°C. The major findings of the study are listed below:

(1) pH dependence of oxygen reduction activity on carbon

The activity of the oxygen reduction decreases with decreasing pH values. The first wave of the polarization curves with respect to reversible hydrogen potential are shown in Figures 1, 2, 3 and 4 for comparison. There is a linear relationship between the pH value and the half wave potential, $E_{1/2}$, the latter decreasing at a rate of approximately 40 mV per decade of H+ concentration. This relationship holds true at both 25°C and 75°C (See Figures 5 and 6). Decrease of exchange current density was also observed as pH value decreased at both temperatures (See Figures 7 and 8).

(2) Carbonate formation in KOH solution does not effect the oxygen reduction activity on carbon:

There was no direct significant effect on the activity as seen from the polarization curves obtained in $CO_3^{=}$ containing KOH solution. Indirectly, however, the formation of carbonate affected the pH value and hence the activity. Also as a secondary effect, an increase in carbonate formation may result in a decrease in the conductivity of the solution.

(3) Reaction sequence:

The plot of i_d/i_r vs $(\omega)^{-\frac{1}{2}}$ for KOH solutions indicated the reaction sequence to be as follows: oxygen reduces to hydrogen peroxide, which is then further reduced to water at higher cathodic polarization.

This may be expressed as:

$$O_2 + 2H^+ \xrightarrow{2e} H_2O_2 \xrightarrow{2e} 2OH^-.$$

The analyses also indicate that no four-electron reduction of oxygen on carbon occurs.

FIGURE 1

THE FIRST WAVE OF THE POLARIZATION CURVES IN 0.1M/0.1M SOLUTIONS AT 25° C

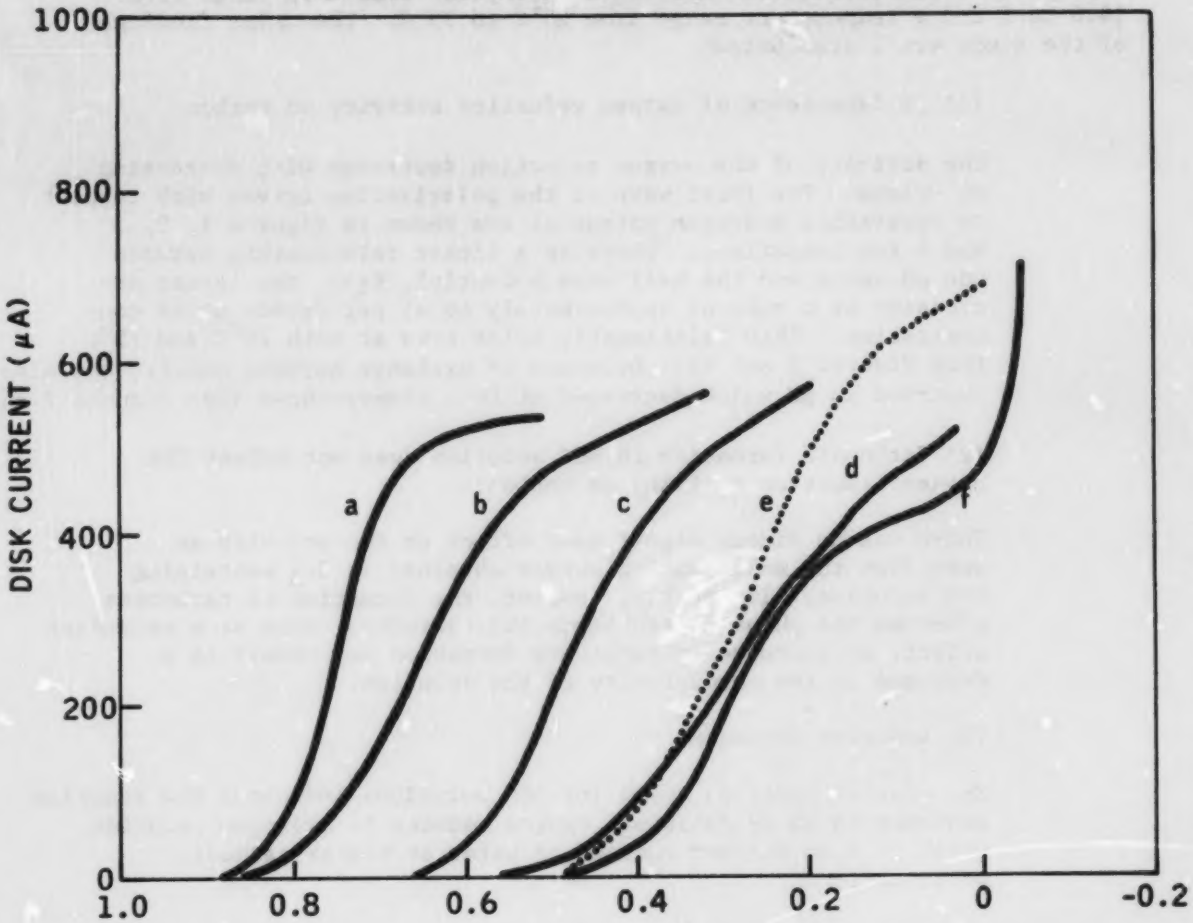

a.	0.1 N KOH	pH = 13
b.	0.1M/0.1 K_2CO_3 - $KHCO_3$	pH = 10.3
c.	0.1M/0.1M K_2HPO_4 - KH_2PO_4	pH = 6.8
d.	0.1M/0.1M KAcO - HAcO	pH = 4.6
e.	0.1M/0.1M KH_2PO_4 - H_3PO_4	pH = 2.1
f.	0.1 N H_2SO_4	pH = 1

FIGURE 2

THE FIRST WAVE OF THE POLARIZATION CURVES IN 0.1M/0.1M SOLUTION AT 75°C

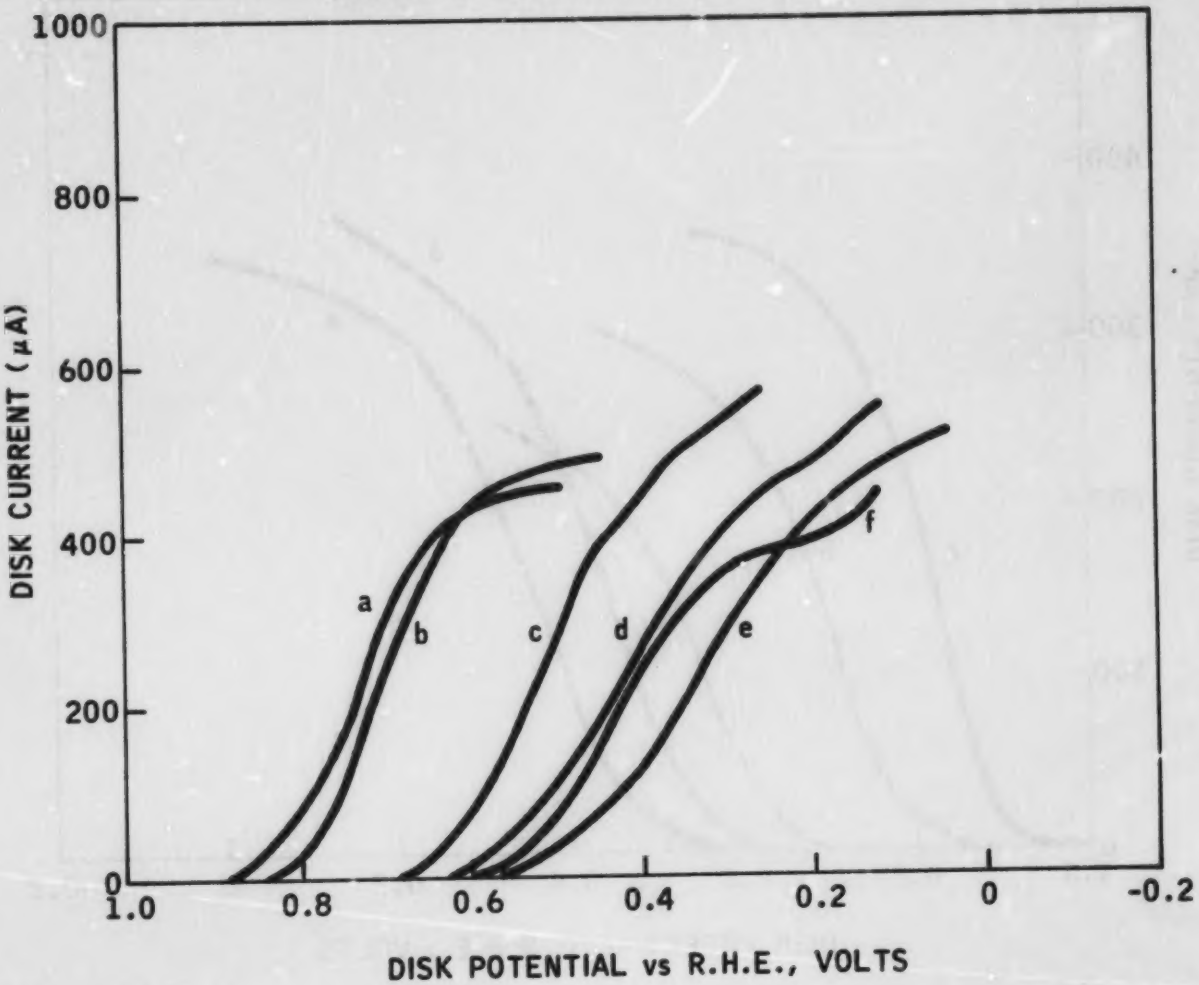

a.	0.1 N KOH	pH = 13
b.	0.1M/0.1M K_2CO_3 - $KHCO_3$	pH = 10.3
c.	0.1M/0.1M K_2HPO_4 - KH_2PO_4	pH = 6.8
d.	0.1M/0.1M KAcO = HAcO	pH = 4.6
e.	0.1M0.1M KH_2PO_4	pH = 2.1
f.	0.1 N H_2SO_4	pH = 1

FIGURE 3

THE FIRST WAVE OF THE POLARIZATION CURVES IN 1M/1M SOLUTION AT 25°C

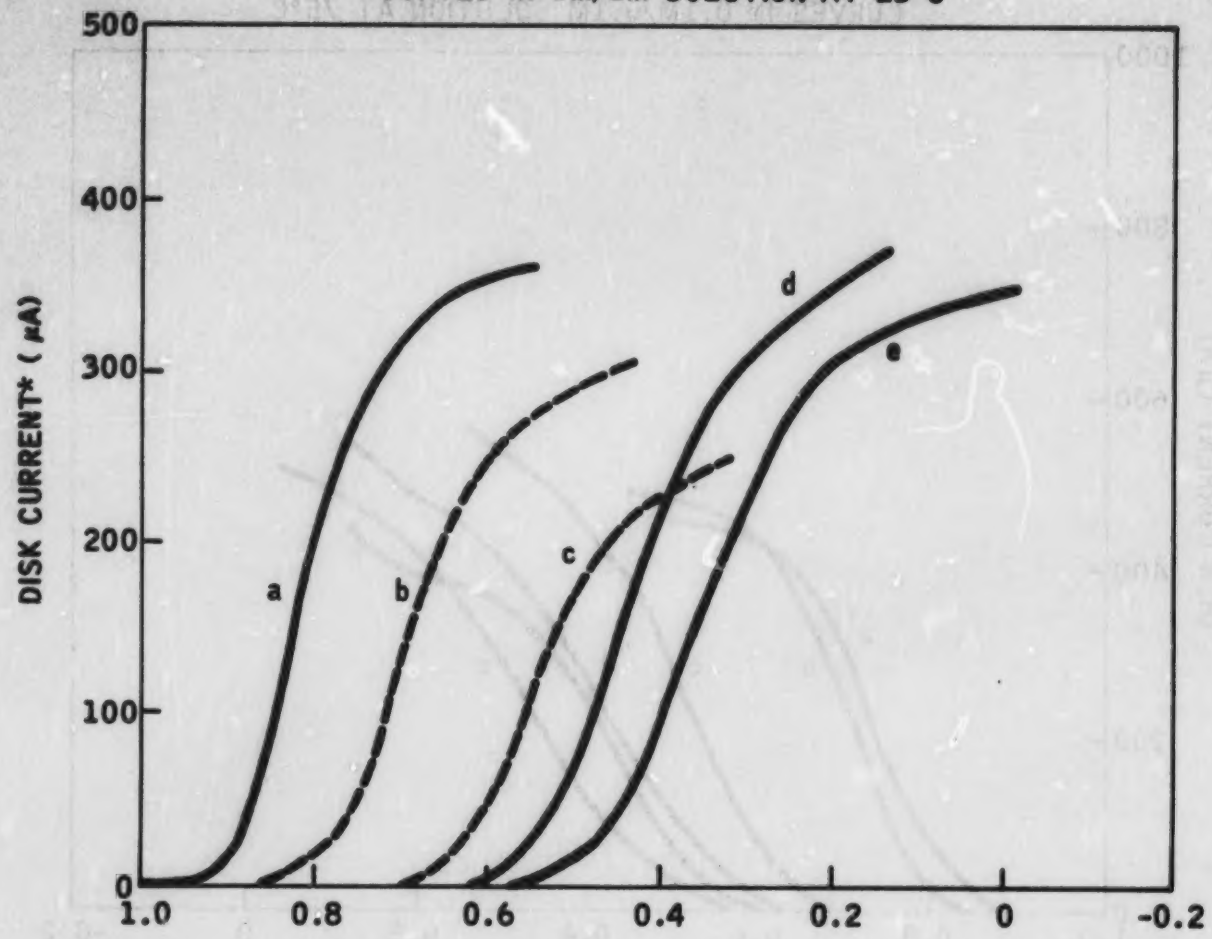

a.	1N KOH	pH = 14
b.	1M/1M K_2CO_3 - KHCO	pH = 10.3
c.	1M/1M K_2HPO_4 - KH_2PO_4	pH = 6.8
d.	1M/1M KAcO - HAcO	pH = 4.6
e.	1M/1M KH_2PO_4 -- H_3PO_4	pH = 2.1

*The current unit for (b) and (c) is half of the scale shown

FIGURE 4

THE FIRST WAVE OF THE POLARIZATION CURVES IN 1M/1M SOLUTION AT 75°C

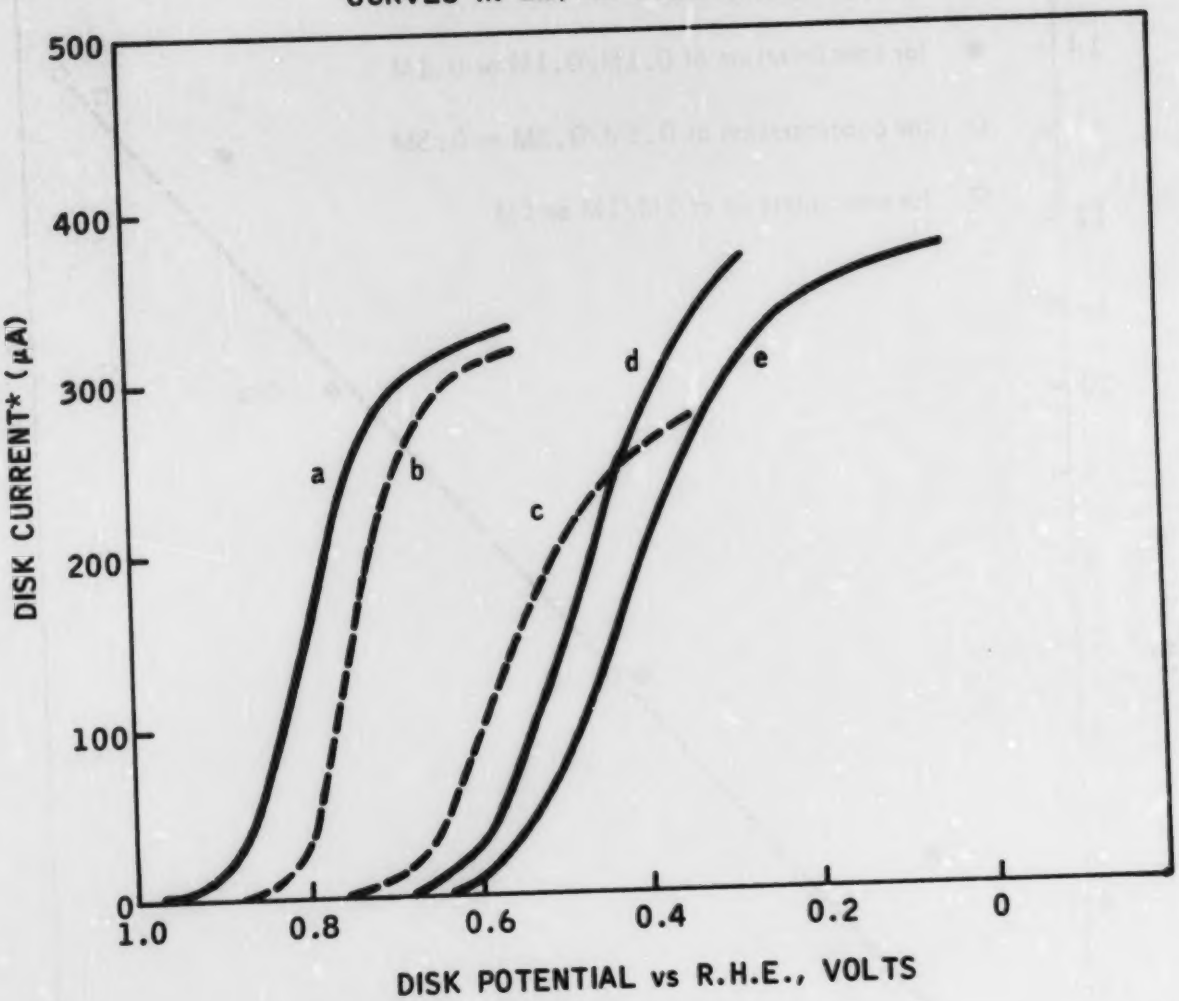

a. 1N KOH
b. 1M/1M K_2CO_3 - $KHCO_3$
c. 1M/1M K_2HPO_4 - KH_2PO_4
d. 1M/1M KAcO - HAcO
e. 1M/1M KH_2PO_4 - H_3PO_4

*The current unit for (b) and (c) is half of the scale shown.

FIGURE 5

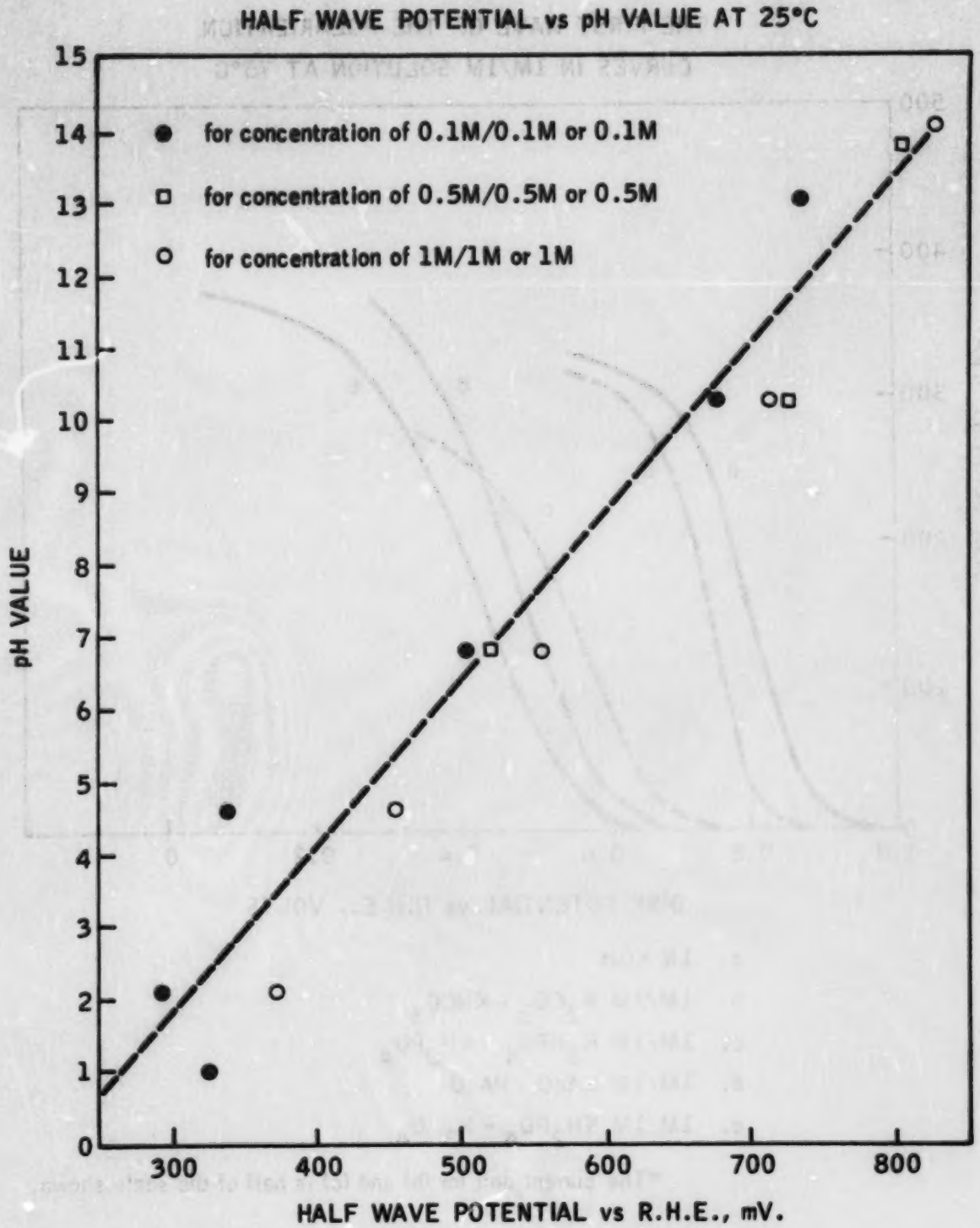
HALF WAVE POTENTIAL vs pH VALUE AT 25°C
for concentration of 0.1M/0.1M or 0.1M
for concentration of 0.5M/0.5M or 0.5M
for concentration of 1M/1M or 1M
pH VALUE
HALF WAVE POTENTIAL vs R.H.E., mV.
0
1
2
3
4
5
6
7
8
9
10
11
12
13
14
15
300
400
500
600
700
800

FIGURE 6

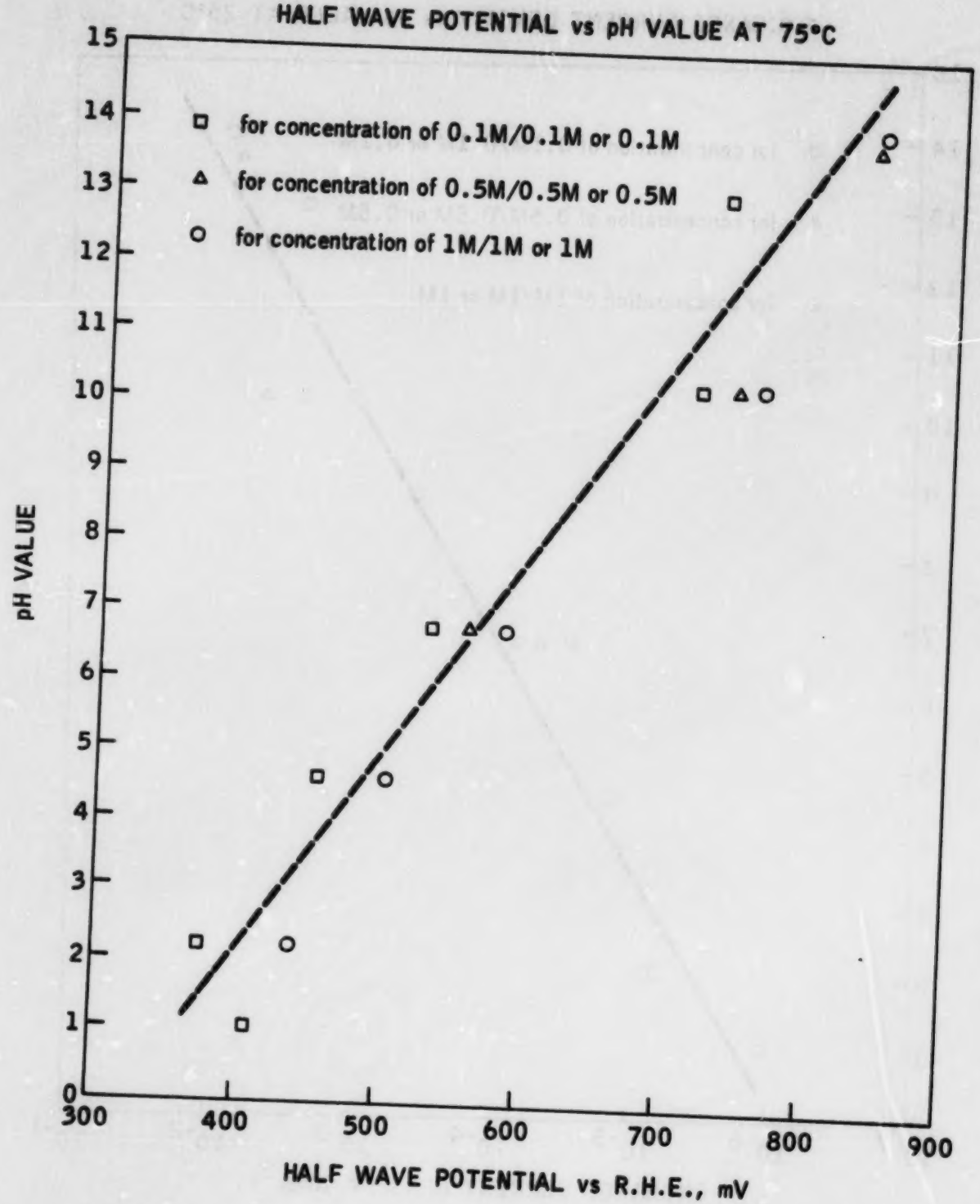
HALF WAVE POTENTIAL vs pH VALUE AT 75°C
for concentration of 0.1M/0.1M or 0.1M
for concentration of 0.5M/0.5M or 0.5M
for concentration of 1M/1M or 1M
pH VALUE
0
1
2
3
4
5
6
7
8
9
10
11
12
13
14
15
300
400
500
600
700
800
900
HALF WAVE POTENTIAL vs R.H.E., mV

FIGURE 7

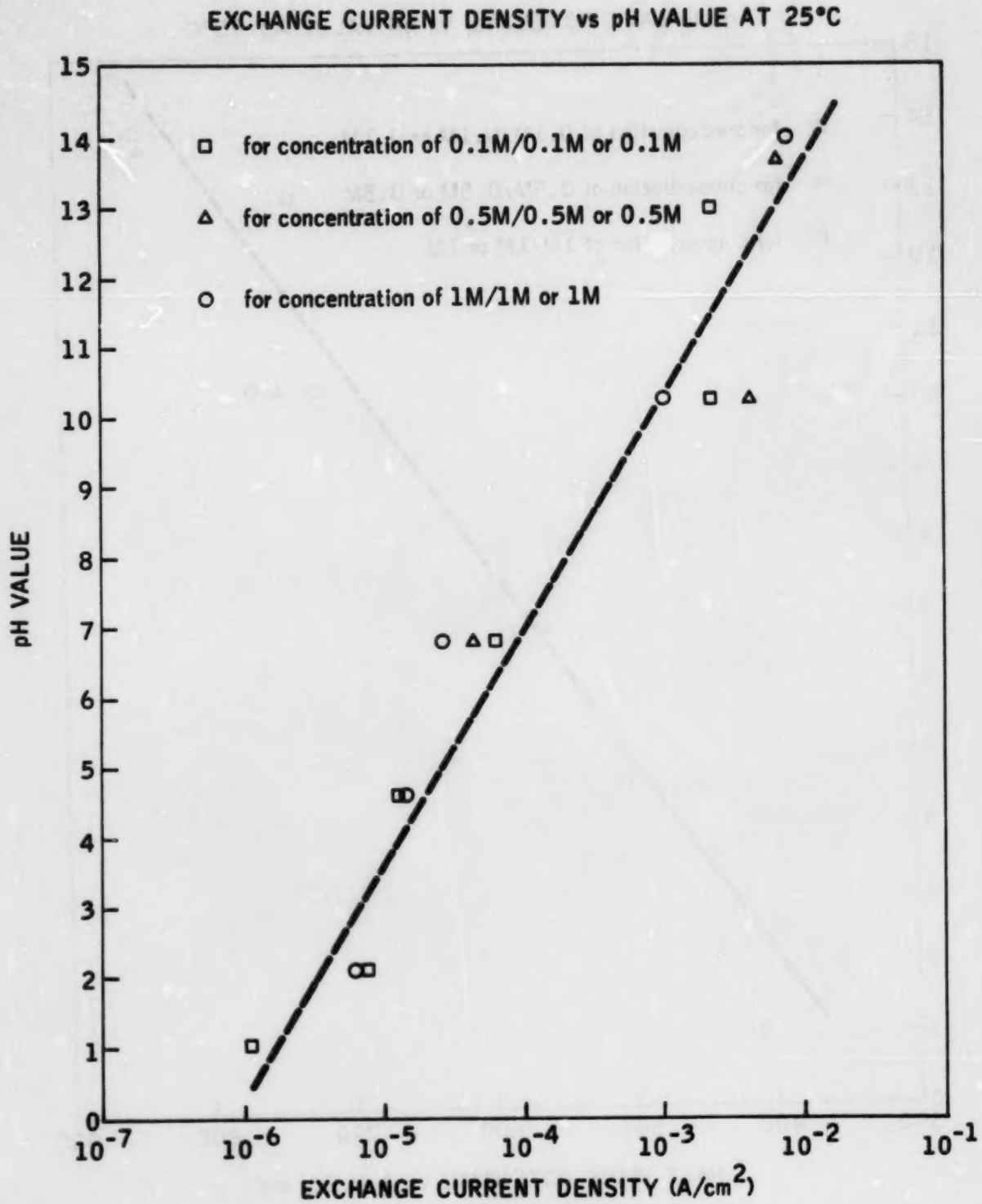
EXCHANGE CURRENT DENSITY vs pH VALUE AT 25°C
for concentration of 0.1M/0.1M or 0.1M
for concentration of 0.5M/0.5M or 0.5M
for concentration of 1M/1M or 1M
pH VALUE
0
1
2
3
4
5
6
7
8
9
10
11
12
13
14
15
10^{-7}
10^{-6}
10^{-5}
10^{-4}
10^{-3}
10^{-2}
10^{-1}
EXCHANGE CURRENT DENSITY (A/cm^2)

FIGURE 8

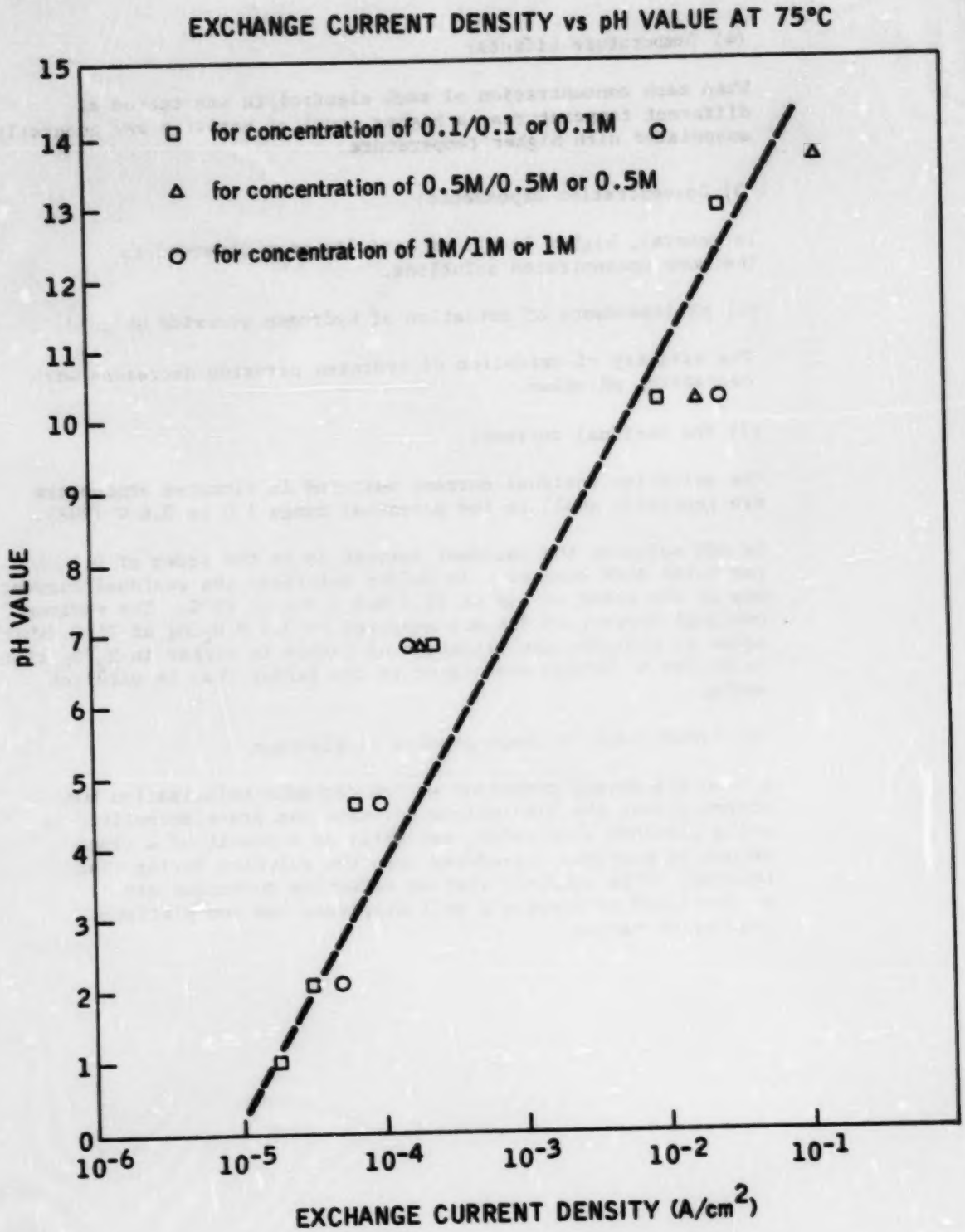
EXCHANGE CURRENT DENSITY vs pH VALUE AT 75°C
for concentration of 0.1/0.1 or 0.1M
for concentration of 0.5M/0.5M or 0.5M
for concentration of 1M/1M or 1M
pH VALUE
0
1
2
3
4
5
6
7
8
9
10
11
12
13
14
15
10-6
10-5
10-4
10-3
10-2
10-1
EXCHANGE CURRENT DENSITY (A/cm2)

(4) Temperature effects:

When each concentration of each electrolyte was tested at different temperatures, a higher level of activity was generally associated with higher temperature.

(5) Concentration dependence:

In general, higher levels of activity were observed in the more concentrated solutions.

(6) pH dependence of oxidation of hydrogen peroxide on gold.

The activity of oxidation of hydrogen peroxide decreases with decreasing pH value.

(7) The residual current:

The oxidation residual current measured in nitrogen atmosphere are generally small in the potential range 1.0 to 0.6 V (RHE).

In KOH solution the residual current is in the order of 0.1μA per total disk surface. In buffer solutions, the residual current was in the order of 1μA at 75°C and 0.5μA at 25°C. The maximum residual current of 4μA was measured in 0.1 M H_2SO_4 at 75°C, which seems to indicate the oxidation of carbon is higher in H_2SO_4 than in buffer solutions and higher in the latter than in alkaline media.

(8) Effects due to trace amounts of platinum:

A complete oxygen reduction at low cathodic polarization was observed when the electrolyte solution was pre-electrolized by using platinum electrodes, evidently as a result of a trace amount of platinum introduced into the solution during that process. This suggests that an effective technique may be developed to prepare a well dispersed and low platinum loading on carbon.

3. CONCLUSION

The catalytic action of carbon is enhanced in an alkaline medium and is progressively retarded as the electrolyte become more acidic. Alkaline medium is therefore the most suitable electrolyte for using carbon alone as the oxygen cathode. The polarization curves obtained in alkaline medium show that 45μA current can be obtained at a polarization of .38V below the theoretical oxygen reversible potential, 1.23V RHE. Double layer capacitance measurements indicate that a 1 cm^2 electrode containing 10 mg of high surface area carbon has 4,000 times the wetted surface area of our rotating graphite disk electrode. By extrapolating the results obtained by rotating disk electrode to the high surface area carbon, it suggests that a completely utilized 10 mg/cm^2 high surface area carbon electrode is capable of delivering 180 mA/cm^2 at 0.38V polarization; e.g. without including other efficiency losses the hydrogen fuel cell could have a cell voltage of .85V and a power density of 140 watts per square foot. Fuel cell power plants for utility applications require a cell voltage of 0.65 to 0.80 volt and a power density of 100 to 200 watts per square foot(6). Therefore, carbon is an acceptable cathode material in alkaline solution, if coupled with a highly efficient hydrogen anode. However, our results show that carbon is a poor catalyst for H_2O_2 reduction (below 0.88V polarization from oxygen equilibrium potential). The concentration of H_2O_2 produced from O_2 reduction will build up in the electrolyte, and the diffusion of H_2O_2 to anode will reduce the efficiency of the H_2 anode. In order to decrease the H_2O_2 concentration in the electrolyte, either a carbon electrode incorporating an effective H_2O_2 reduction catalyst or an electrolyte contained soluble H_2O_2 decomposition catalyst is necessary. Since the carbon electrode can only be used in alkaline electrolyte to achieve the power density needed, the essential problem of carbonate and bicarbonate formation by using organic or reformed -CO_2- containing fuel still remains to be overcome.

Though carbon by itself may not be useful as a catalyst, its use as a support is unquestionably of great importance due to its high surface area and electrical conductivity. Also, if there is bifunctional catalytic action and favorable metal-carbon interaction, one could have increased overall activity. The fact that this study found the stability of carbon to decrease substantially with decreasing pH values, but overall is still excellent when compared to other known possible supports, is very useful information. The above points indicate the necessity of studying carbon as an electrode material.

We reiterate the observation of substantial improvement in catalytic action for oxygen reduction due to the presence of extremely small quantities of platinum introduced into the system just by pre-electrolysis of the electrolyte with platinum electrodes. This favorably underscores the points made previously and indeed suggests that an effective technique can be developed to prepare a well dispersed, low platinum loaded carbon cathode.

The dependence of the catalytic activity of carbon on pH is most probably be due to the concentration of H^+. The half wave potential of the oxygen reduction reaction vs pH value plot would have a slope of 59 mV/decade, if the reaction is not dependent on H^+ concentration; and it would have a zero slope if the reaction has a first order dependance on H^+ concentration. The slope obtained in this study was approximately 40 mV/decade, and it suggests the rate dependence of a fractional order of H^+ concentration. One possible explanation is the occurrence of two slow irreversible steps; one containing H^+ such as

$$*O_2^- + H^+ \longrightarrow *HO_2,$$

the other being $* + O_2 + 2e \longrightarrow *O_2^-$ and the rest of the steps being in quasi-equilibrium. Here, * indicates the surface. However, effects such as the influence of solvent (electrolyte) on species absorbed on carbon and hence the effect on activated complexes could be important and should be given further consideration in more detailed future work. Fundamentally, the study of solvent-solid catalyst interaction is important in order to be able to understand and hopefully predict catalytic activity. The critical steps, from among the large number of elementary steps which could take place on the surface, have been reported (7). These steps can be elucidated with more confidence using isotope studies (D^+ and O^{18}) coupled with kinetic parameters such as those obtained here and with which we have made some mechanistic prediction.

4. GENERAL DISCUSSION

4.1 Fuel Cell

A fuel cell is a device for continuously converting chemical energy into electrical energy through electrochemical reactions. A fuel cell requires two electronic-conducting electrodes separated by an electrolyte. Fuel is oxidized at the anode furnishing electrons to an external circuit, while the oxidant accepts electrons from the cathode and is reduced. Simultaneously, an ionic current in the electrolyte completes the circuit. In a typical hydrogen-oxygen fuel cell the following reactions take place:

Anode: $H_2 + 2OH^- \longrightarrow 2H_2O + 2e$

Cathode: $\frac{1}{2} O_2 + H_2O + 2e \longrightarrow 2OH^-$

Fuel cell: $H_2 + \frac{1}{2}O_2 \longrightarrow H_2O$

The theoretical cell potential, E, can be predicted from the molar free energy, ΔG, of the cell reaction:

$$\Delta G = -nEF$$

where n is the number of electrons per molecule of fuel that is oxidized, and F is the Faraday constant.

4.2 Polarization Curve

When current is drawn from an electrochemical cell, the terminal voltage of the cell decreases from that which would be anticipated thermodynamically. This phenomenon is called polarization. This decrease in cell voltage reflects not only the potential drop cause by resistance of the circuit and the fuel concentration gradient within the cell, but also potential losses associated with irreversibility of various process at the electrode-solution interfaces. These deviations in the potentials of the electrodes from the values predicted thermodynamically are referred to as electrode polarization. These current vs potential plots are called polarization curves. The reversibility of a given electrode reaction, and therefore the electrode polarization, depends on the electrode material and operating conditions, such as temperature and electrolyte concentration. By studying the behavior of the polarization curves, the nature of the electrode reaction can be determined. Several parameters, such as the half wave potential $E_{\frac{1}{2}}$, the exchange current density, i_o, and the Tafel slope, have been used for the polarization behavior studies. The half wave potential, which is defined as the potential where the current equals half of the diffusion-limited current, has often been used for simple comparison for the reversibility of the electrode reaction. Definitions of the other parameters are discussed below.

4.3 Butler-Volmer Equation and Tafel Line

The electrode polarization may generally be expressed by the well-known Butler-Volmer equation as

$$i = i_o \left[e^{\vec{\alpha} F\eta/RT} - e^{-\vec{\alpha} F\eta/RT} \right] \qquad (2)$$

Here, i, the reaction current, is a measure of the reaction rate; i_o, the exchange current density, is the current flow in any one direction at equilibrium per unit electrode area; η is the overpotential which is defined as the potential difference between the electrode potential and equilibrium potential; α and α are the transfer coefficients. When the overpotential, η is large enough (approximate > 0.1V), one of the terms in Eq.(2) becomes negligible compared to the other. The equation is, therefore, approximately

$$i \simeq i_o \, e^{\vec{\alpha} F\eta/RT} \text{ or } -i_o \, e^{-\vec{\alpha} F\eta/RT} \qquad (3)$$

By taking logarithms of this equation, the Eq. (3) can be reduced into the commonly-used Tafel equation $\eta = -\frac{RT}{\alpha F} \ln i_o + \frac{RT}{\alpha F} \ln i$.

When η values are obtained at various currents, it is possible to obtain linear η vs. log i plots. Such η vs. log i plots are refered to as Tafel lines. The slope of these Tafel lines provides a means of determing the transfer coefficient α, the transfer coefficient consists of the parameter of the fundamental reaction steps and the rate-determined steps. An analysis of the Tafel slope of a polarization curve will therefore be of primary importance in mechanism determination. The exchange current densities can be obtained by extrapolating the Tafel lines to $\eta = 0$. The exchange current densities reflect the kinetic properties of the particular electrode interfacial systems concerned.

4.4 Rotating Ring-Disk Electrode

The rotating ring-disk electrode was used to study the oxygen reduction mechanism. An end on view of such electrode is shown in Figure 9. Here we have two active electrodes: the central disk electrode and the ring electrode. These electrodes are separated by a narrow insulation. The studied reaction is carried out on the disk electrode. Any intermediates which are not firmly bound to the electrode may diffuse from the electrode into the solution. If the electrode is rotating, the solution adjacent to the electrode will acquire a convictive and radial motion (See Figure 10). This will tend to carry the intermediates from the region of the disk past the ring electrode. The intermediate can then be detected at the ring. The collecting efficiency, defined as the ratio of the intermediate produced at the disk detected by the ring to the total intermediate produced at disk, is independent of the rotation speed and the reaction. By examining the simultaneously measured disk and ring currents, the reaction mechanism can therefore be studied.

FIGURE 9

END VIEW OF ROTATING RING-DISK ELECTRODE

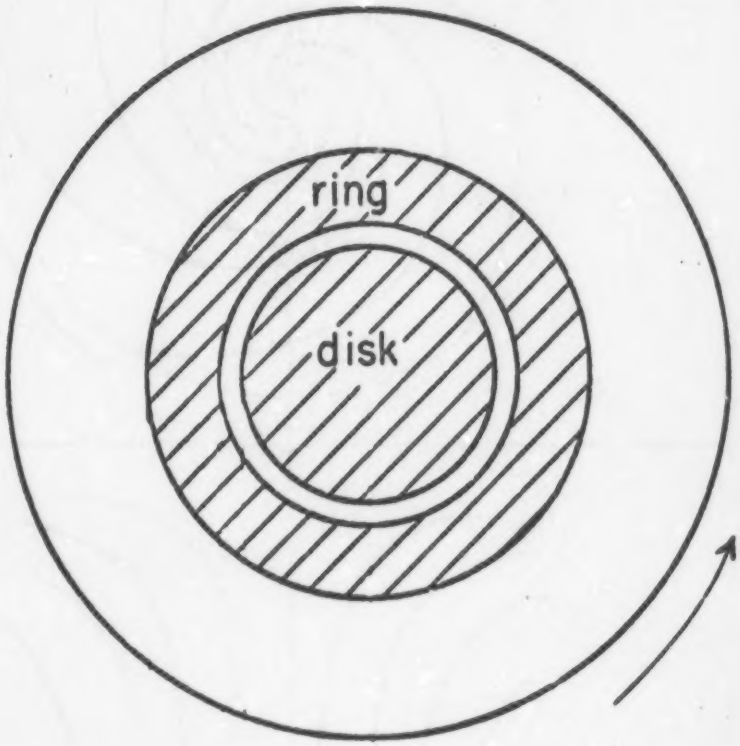

FIGURE 10

THE FLOW PATTERN OF A
ROTATING DISK SHOWING STREAMLINES

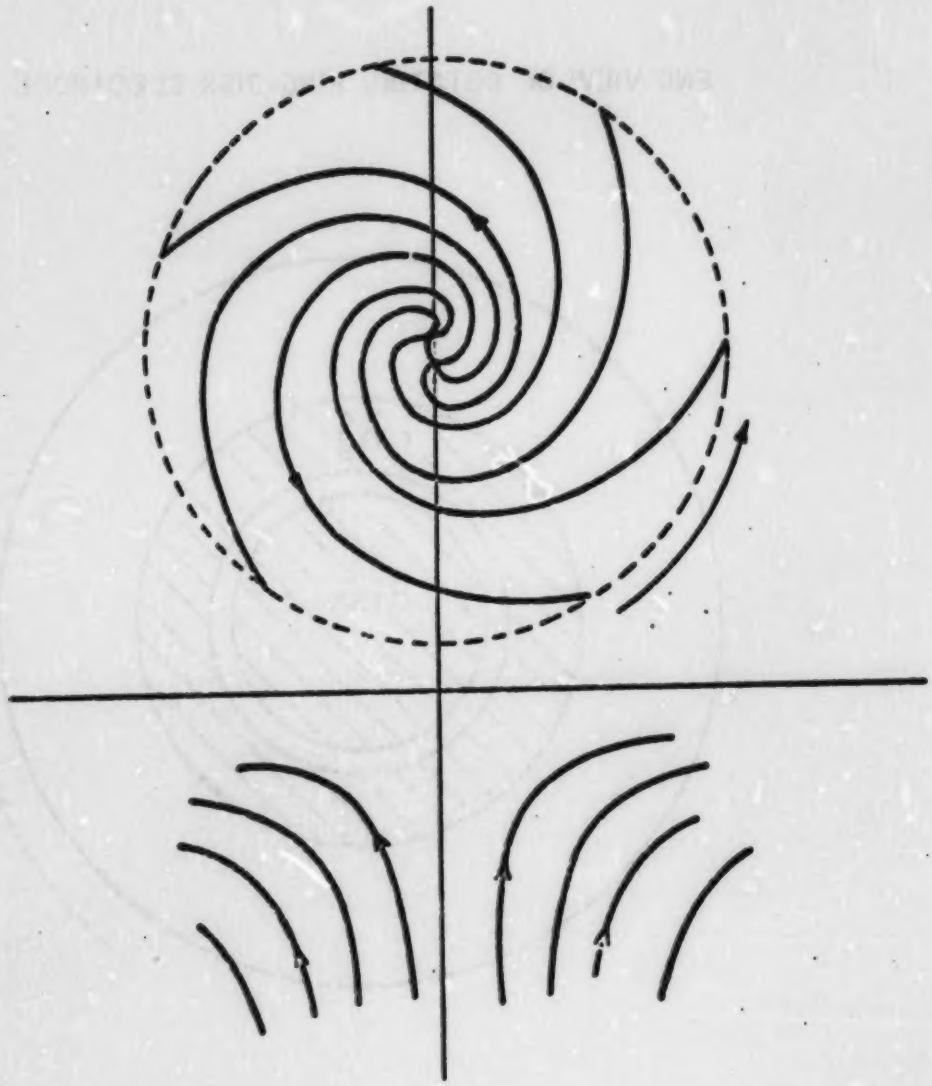

5. EXPERIMENTAL METHOD

The following set of experiments were carried out for each electrolyte concentration and at each temperature (25°C and 75°C, and in some cases 50°C):

a. In O_2 saturated electrolyte, the dependence of the cathodic current and the hydrogen peroxide oxidation current on disk potential were simultaneously recorded, at three different rotating speeds: 500 RPM, 1000 RPM and 2000 RPM.

b. Polarization curves were taken at 1000 RPM before and after 2 drops of 3% H_2O_2 are added to the electrolyte in order to confirm the potential dependence of H_2O_2 reduction on carbon.

c. Residual current, which is the current measured with the absence of oxygen, was determined in a nitrogen saturated electrolyte.

The measurements were always taken after several sweeps between hydrogen and oxygen evolution potentials. By doing so, better reproducibility was obtained and little hysteresis was observed on the reversed scan, which may be due to the slow change of the electrode surface state caused by scanning potential.

Due to the pH change of the electrolyte and a corresponding change in the reversible hydrogen potential, the recorded sweeps were adjusted to the suitable range of potentials. The ring potentials were also adjusted in order to obtain the maximum hydrogen peroxide oxidation current without the interference of the oxygen evolution current. The starting potentials for the recorded sweeps and the ring potential for different pH values are listed in Table 1.

The experimental results reported in this work were obtained by the slow sweep voltammetry technique used in conjunction with rotating ring and disk electrodes. The block diagram of the potentiostatic ring and disk circuit is given in Figure 11. Current-voltage polarization curves were obtained by slow linear sweep voltammetry with a Princeton Applied Research potentiostat (Model 173) and a universal programmer (Model 175) as a source of scanning voltage. The ring potential was controlled by a home built potentiostat. An X-Y-Y' plotter (Esterline Angus 540) was used to record the currents as a function of disk potential. All results reported here are for a scan rate of 5 mv/sec. Slower scanning rates also have been examined but no significant differences were found.

The disk electrode studied (see Figure 9) was made out of a Carbone Corporation 5890 grade graphite (density 1.85 g/cm^3). Instead of platinum, 99.999% purity gold from Engelhard Industries was used for the ring and the counter electrode construction in order to prevent platinum contamination. The ring-disk electrodes were molded together by Delta Cast 153 ETC epoxy from Wakefield Engineering Inc. The Delta Cast 153 ETC has excellent chemical resistance for the range of electrolytes we have studied.

Table I

Electrochemical Potentials Related to Oxygen Reduction in Various Solutions

Solution	pH	RHE vs SCE(mv)	Recording Sweep Starting Potential (SCE)	Equilibrium Potential vs RHE $O_2+2H^+ \rightleftharpoons H_2O_2$ used in this report			Ring Potential used in Our Experiments vs. SCE
				25°C	50°C	75°C	
4N KOH	14.6	-1105	0	769	758	748	0
2N KOH	14.3	-1087	0	760	749	739	0
1N KOH	14	-1068	0	751	740	730	0
0.5 KOH	13.7	-1049	0	742	731	721	0
0.1 KOH	13	-1009	0	721	711	701	0
2N/2N KOH-K_2CO_3	14.57	-1100	0	769	758	748	0
1:1 K_2CO_3 - $KHCO_3$	10.3	-850	+100	682	657	633	+350 mV
1:1 K_2HPO_4 - KH_2PO_4	6.8	-643	+200	682	657	633	+570 mV
1:1 KAcO- HAcO	4.6	-513	+250	682	657	633	+1.02 V
1:1 KH_2PO_4 - H_3PO_4	2.1	-365	+400	682	657	633	+1.35 V
0.1N H_2SO_4	1	-300	+450	682	657	633	+1.50 V

FIGURE 11

CIRCUIT DIAGRAM FOR ROTATING
RING-DISK ELECTROCHEMICAL MEASUREMENTS

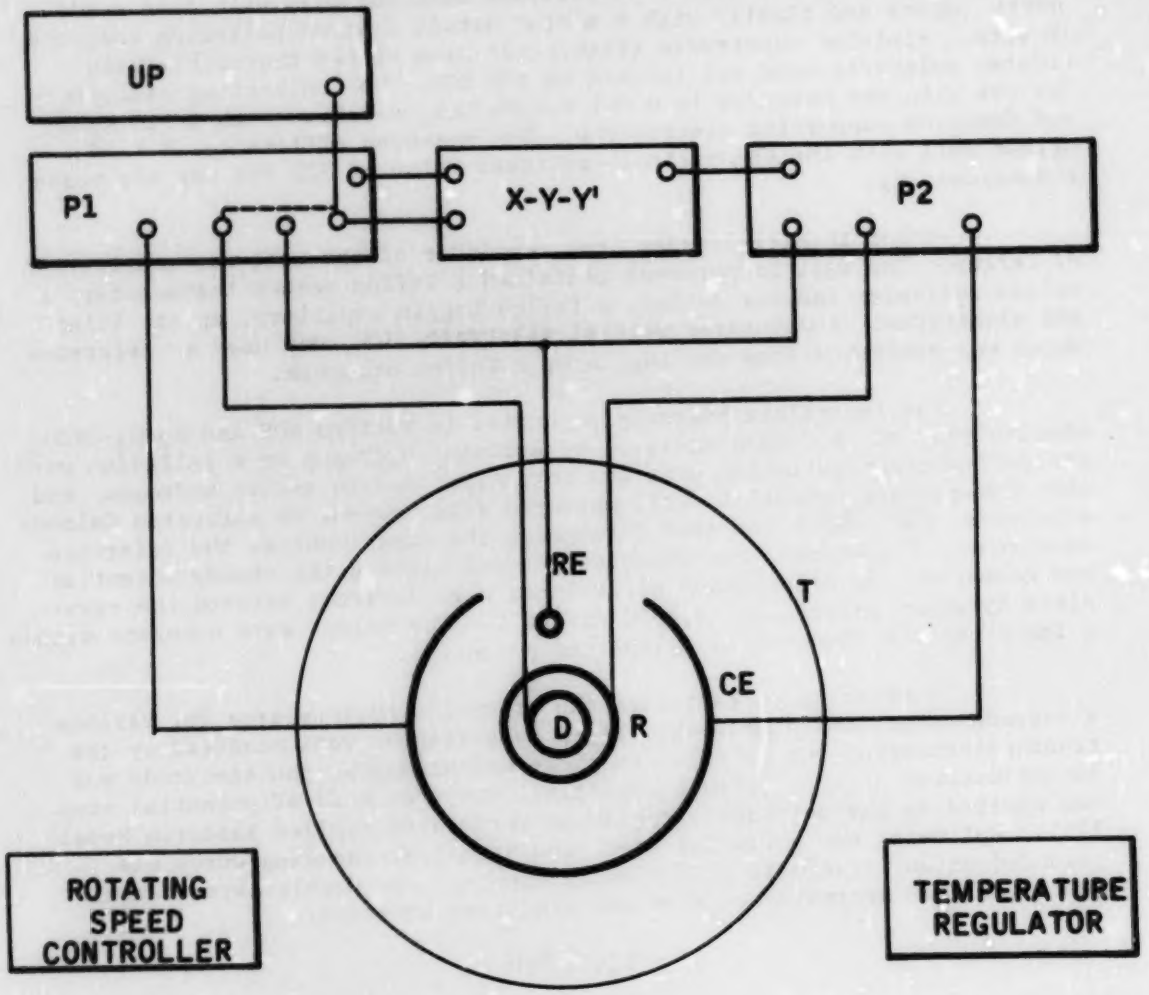

CE	Counter Electrode
D	Disk Electrode
P1	Potentiostat for the Disk Electrode
P2	Potentiostat for the Ring Electrode
R	Ring Electrode
RE	Saturated Caromel Electrode, SCE.
T	Teflon Cell
UP	Universal Programmer
X-Y-Y'	X-Y-Y' Recorder

This epoxy was chosen mainly for its low thermal expansion coefficient (1.8×10^{-5} cm/cm/°C) relative to other commonly used materials. The molding technique was adapted to prevent possible leakage due to differential expansion for elevated temperature study. After the machining of molded electrodes, the electrode surfaces were polished with fine grade emery papers and finally with 6 micron Matadi diamond polishing compound in situ. Finished electrodes (Figure 12) were rinsed thoroughly with diluted sulphuric acid and leached in 45% KOH. The collecting efficiency for the ring was measured in 0.001 M $K_3Fe(CN)_6$ solution with 1M:1M K_2CO_3 and $KHCO_3$ as supporting electrolyte. The measured efficiency, N = 33%, agreed well with the theoretical predicted value of 32% for our electrode dimensions (8).

Other than electrodes, the remainder of the cell was constructed of Teflon. The cell compartment contained a Teflon coated thermometer, a reflux condenser and air outlet, a Teflon Luggin capillary, an air inlet and electrodes. A saturated Calomel electrode, SCE, was used as reference, which was separated from the Luggin by a Teflon stopcock.

The reversible hydrogen potential in various KOH and K_2CO_3-$KHCO_3$ electrolytes at 75°C were measured by evolving hydrogen on a palladium wire. The palladinized palladium wire was potentiostated to evolve hydrogen, and the open-circuit potentials were measured with respect to saturated Calomel electrode, SCE, which was used throughout the experiment as the reference electrode. The process was repeated several times until steady potential was measured. No significant differences were detected between the reversible hydrogen potentials at 75°C and 25°C. The values were accurate within a few mV to the theoretical calculated potential.

In order to characterize the effective surface area for various electrode conditions, the double layer capacitances were measured by the transient-charging-curves (9). In these measurements, the electrode was potentiostated at open circuit potential, and then a 25 mV potential step was applied by the universal programmer (Princeton Applied Research Model 175). Following the potential step, the transient charging curve was recorded on an Techtronix 5103 N oscilloscope. The double layer capacitence was then approximated from the transient equation:

$$I = I_o e^{-t/R_e C}$$

here I_o is the peak current at the step, C is the double layer capacity, and R_e is the effective resistance of the circuit, which can be directly obtained from $R_e = \frac{\Delta V}{I_o}$, where ΔV is the applied potential step.

FIGURE 12

ROTATING RING-DISK ELECTRODE ASSEMBLY

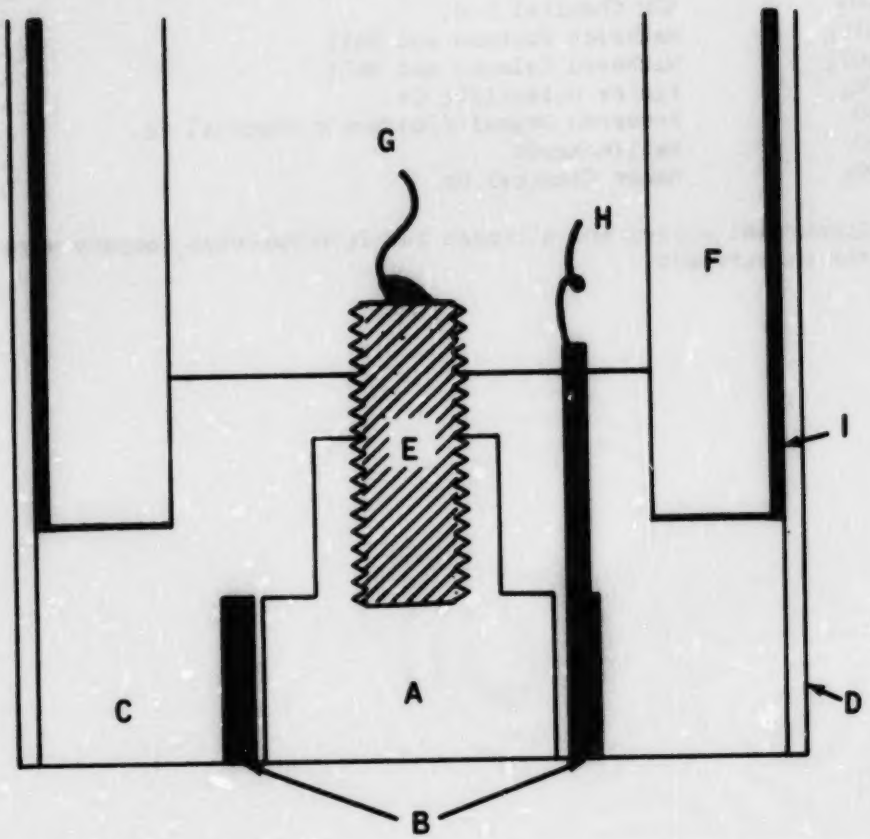

A. Graphite disk (O.D. .483 cm, Area .183 cm^2)
B. Gold ring (I.D. .531 cm, O.D. .635 cm)
C. Epoxy holder and spacer
D. Shrinkable Teflon tubing
E. Stainless steel screw
F. Stainless steel rotating shaft
G. Disk electrical connection
H. Ring electrical connection
I. Epoxy seal

Except where otherwise noted, the electrolytes were prepared from following listed chemicals and distilled deionized water.

Chemical	Manufacture	Purity Grade
KOH	Mallinckrodt	Analytical Reagent
$KHCO_3$	Carlo Erba Chemical, Italy	Analytical Reagent
K_2CO_3	BDH Chemical Ltd.	Analytical Reagent
K_2HPO_4	Matheson Coleman and Bell	A.C.S. Reagent
KH_2OP_4	Matheson Coleman and Bell	A.C.S. Reagent
H_3PO_4	Fisher Scientific Co.	A.C.S. Reagent
KAcO	Research Organic/Inorganic Chemical Co.	Analytical Reagent
HAcO	Mallinckrodt	Analytical Reagent
H_2SO_4	Baker Chemical Co.	Ultra High Purity

Commercial oxygen and nitrogen gas from Matheson Company were used for the measurement.

6. RESULTS AND DISCUSSION

The potential and current relationships for electrochemical reduction of oxygen on carbon were obtained over a wide range of pH values (from 4N KOH to 0.1N H_2SO_4), electrolyte concentrations and temperatures. The results are grouped into the various chemical compositions of the electrolyte and discussed in the following five subsections. The correlations between all the measurements are summarized and concluded at the end of this section.

6.1 Studies in Potassium Hydroxide

The electrochemical reduction of oxygen on carbons in KOH solution are practically important, owing to the high conductivity of the OH^- ion and good oxygen reduction activity observed on high surface carbon. Five different KOH concentrations, 0.1, 0.5, 1.0, 2.0 and 4.0 N, were investigated. The information obtained is discussed in the following separate subsections.

6.1.1 Polarization Curves

The dependence of the cathodic currents and the hydrogen peroxide oxidation currents on disk potential were simultaneously recorded for the various KOH concentrations mentioned above. For each concentration, data were obtained at 25°C, 50°C and 75°C. In all KOH measurements, the recorded sweep was started at 0 mV SCE (the theoretical hydrogen reversible potential in 1N KOH is - 1.07 V SCE) and polarized to hydrogen evolution.

For each chosen concentration and temperature, measurements were taken at three different rotating speeds, 500, 1000 and 2000 RPM. A typical result obtained for 0.1N KOH at 25°C is presented in Figure 13. The curves are designated by rotating speed and solid and dotted line indicate the disk or the ring current, respectively. In general, the disk current vs its potential plot present two distinct waves which are noted to be of equal height. The first wave is expected to be the reduction of oxygen to hydrogen peroxide; the second is the further reduction of hydrogen peroxide to water or hydroxide ion. This expected reaction sequence is consistant with the hydrogen peroxide oxidation current simultaneously measured on the ring.

The polarization curves obtained in 0.5N KOH and some of the 1N KOH solutions, (see Figure 14, obtained in 0.5N KOH) show a maximum before reaching the first plateau. These maximums were also observed in Morcos and Yeager's study of pyrolytic graphite(4). The heights of the maximums varied somewhat during separate measurements. Nevertheless, the increase in the height of the disk current peak always corresponded with a proportional decrease in the ring current level. It is clearly indicated that the additional current is contributed by the further reduction of H_2O_2 formed in the first step of oxygen reduction, instead of the explanation given by Morcos and Yeager as that secondary effect associated with a decrease in electrocatalytic activity of the electrode surface at more cathodic potentials after passing through the maximum. We believe this additional current is due to the oxidation state of the carbon surface or some trace impurity in the electrolyte preferentially adsorbed on the electrode surface at that potential which catalized the chemical decomposition or further reduction of H_2O_2. For unknown reasons, the reactions are more sensitive at these medium concentrations of 0.5N and 1N.

FIGURE 13

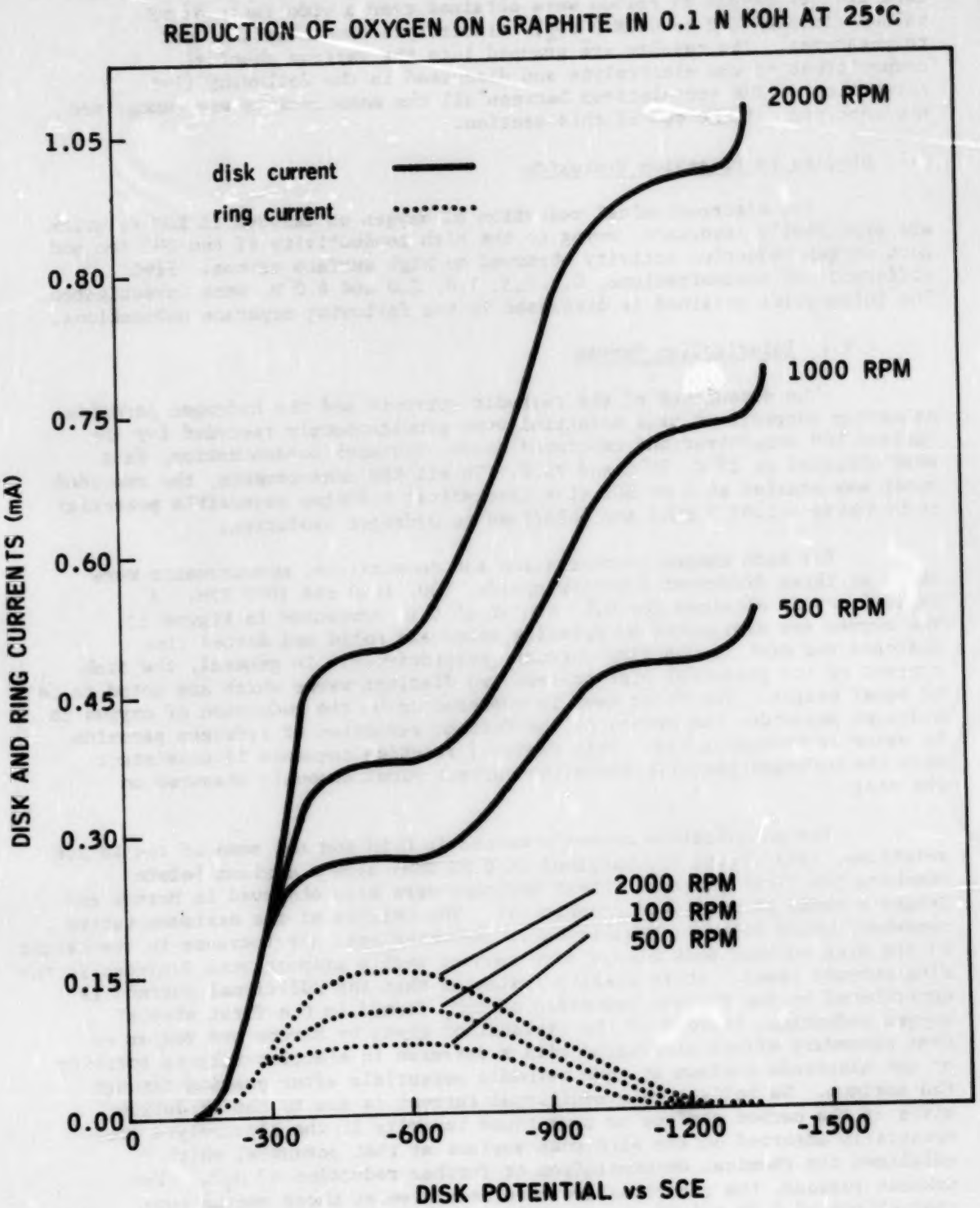
REDUCTION OF OXYGEN ON GRAPHITE IN 0.1 N KOH AT 25°C
2000 RPM
1000 RPM
500 RPM
disk current
ring current
2000 RPM
100 RPM
500 RPM
1.05
0.80
0.75
0.60
0.45
0.30
0.15
0.00
0
-300
-600
-900
-1200
-1500
DISK AND RING CURRENTS (mA)
DISK POTENTIAL vs SCE

FIGURE 14

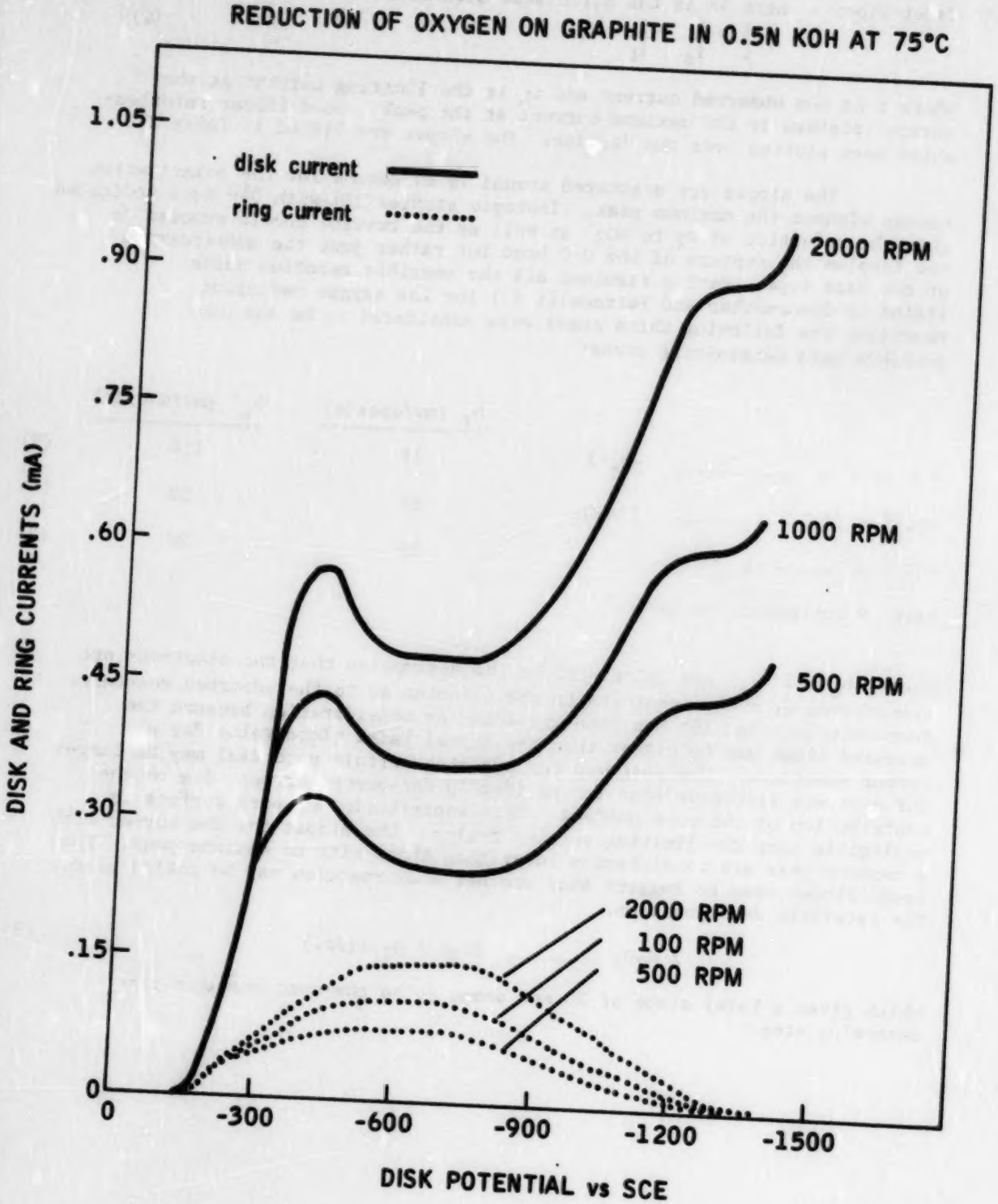
REDUCTION OF OXYGEN ON GRAPHITE IN 0.5N KOH AT 75°C
1.05
.90
.75
.60
.45
.30
.15
0
disk current
ring current
2000 RPM
1000 RPM
500 RPM
2000 RPM
100 RPM
500 RPM
DISK AND RING CURRENTS (mA)
0
-300
-600
-900
-1200
-1500
DISK POTENTIAL vs SCE

The polarized potentials were plotted vs log i_a to approximate the Tafel slopes. Here i_a is the calculated activation current via the formula

$$\frac{1}{i} = \frac{1}{i_a} + \frac{1}{i_L} \qquad (4)$$

where i is the observed current and i_L is the limiting current at the current plateau or the maximum current at the peak. Good linear relationships were plotted over two decades. The slopes are listed in Table 2.

The slopes are scattered around 79 mv/decade for the polarization curves without the maximum peak. Isotopic studies (10) with O^{18} have indicated that the reduction of O_2 to HO_2^- as well as the reverse anodic process do not involve the rupture of the O-O bond but rather just the modification of the bond type. Having examined all the possible reaction paths listed by Gnanamuther and Petrocelli (7) for the oxygen reduction reaction, the following three steps were considered to be the most probable rate determining steps:

	b_c (mv/decade)	b_c' (mv/decade)	
$* + O_2 + 2e \longrightarrow *O_2^{-2}$	59	118	(5)
$*O_2^{-2} + 2H_2O \longrightarrow 2*H_2O_2$	30	59	(6)
$*O_2^- + H^+ \longrightarrow *HO_2$	59	79	(7)

here, * represents surface,

where $-b_c$ and $-b_c'$ are calculated on the assumption that the electrons are transferred from the substrate to the solution or to the adsorbed reactants respectively. Eq. (6) has been included for consideration because the measured slope may be higher than the actual Tafel slope value for a porous electrode. The observed current at a certain potential may be larger for a porous electrode than for an ideally non-porous carbon, due to the contribution of the pore surface. This contribution of pore surface is negligible near the limiting current region. The slopes for the curves with a maximum peak are consistantly lower than those with no maximum peak. The lower slopes seem to suggest that another slow reaction may be taking place. The catalytic decomposition,

$$2\,H_2O_2 \longrightarrow 2H_2O + O_2\ (ads.) \qquad (8)$$

which gives a Tafel slope of 30 mv, seems to be the most probable rate determing step.

Some of the additional electrochemical parameters derived from these polarization curves, such as exchange current density, half wave potential and the potential at which H_2O_2 starts to undergo further reduction, are also listed in Table 2. These parameters characterized the behavior of the oxygen reduction reaction under various conditions and were used for the later comparison in section 3.5.

The exchange current densities are obtained by extrapolating the approximated Tafel line to the reversible potential of electrochemical reduction of O_2 and oxidation of H_2O_2. The reversible potentials are affected by the dissociation of $H_2O_2 \rightleftharpoons H^+ + HO_2^-$, which has a dissociation constant of $10^{-11.6}$. Therefore, the equation, E_o (at 25°C) = 0.338 + 0.0295 pH (RHE), was used in alkaline region to obtain the reversible potentials. To evaluate the current density at 50°C and 75°C, the approximated equations E_o (at 50°C) = 0.327 + 0.0295 pH and E_o (at 75°C) = 0.317 + 0.029 pH (RHE) were used to obtain the reversible potential due to the temperature correction of the free energy and the dissociation constant of H_2O_2. The half wave potentials are dependant on the rotating speed and the area of the rotating disk electrode. However, under the defined conditions, the half wave potential is a good criteria for the electrochemical polarization comparison. The average values of three rotating speeds, 500, 1000 and 2000 RPM are listed on Table 2.

6.1.2 The plot of i_d/i_r vs $(\omega)^{\frac{1}{2}}$ and reaction mechanism

The oxygen reduction reaction sequence can be examined by plotting the disk to ring current ratio, i_d/i_r, versus $\omega^{\frac{1}{2}}$, where ω is the angular velocity of the electrode. As we mentioned before, a general scheme of oxygen reduction can be expressed as

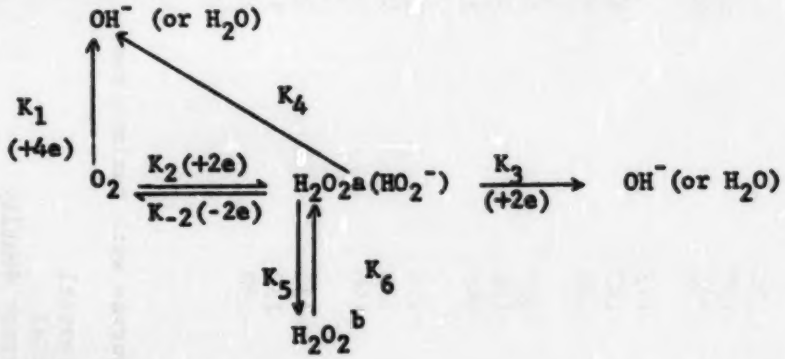

(1)

The reaction rate constant for each step is designated by the subscribed number, respectively.

Table 2

Parameters Involved in the Determination of the Oxygen Reduction Reaction Activity in KOH Solutions

Concentration	Temperature	Eo (a) (mv vs SCE)	Slope of Potential vs log ia plot (mV/decade)	$E_{\frac{1}{2}}$ (b) (mV vs SCE)	(mv vs RHE)	io (c) (A/cm^2)	$E_{H_2O_2}$ (d) (mV vs SCE)
4N	75°C	-150	64	-242	863	1.4×10^{-2}	-750
pH=14.6	50°C	-150	85	-251	854	5×10^{-3}	-750
	25°C	-160	86	-252	853	3×10^{-3}	-800
2N	75°C	-172	72	-242	845	2×10^{-2}	-700
pH=14.3	50°C	-183	92	-278	809	3×10^{-3}	-840
	25°C	-182	95	-294	793	2×10^{-3}	-900
1N	75°C	-135	76 (35)*	-195	872	1.2×10^{-2}	-840
pH=14	50°C	-150	59 (45)*	-202	866	1.5×10^{-2}	-860
	25°C	-140	94 (60)*	-230	838	7×10^{-3}	-860
0.5N	75°C	-135	52*	-203	840	1.7×10^{-1}	-800
pH=13.7	50°C	-135	62*	-212	837	8×10^{-2}	-820
	25°C	-140	77*	-240	809	6×10^{-3}	-800
0.1N	75°C	-130	100	-280	729	3×10^{-3}	-700
pH=13	50°C	-130	81	-266	743	5×10^{-3}	-560
	25°C	-130	77	-276	733	2×10^{-3}	-600

* For the polarization curves with maximum peak.

(a) E_o, Zero current potential
(b) $E_{\frac{1}{2}}$, half wave potential
(c) io, the exchange current density
(d) $E_{H_2O_2}$, the potential where H_2O_2 starts to undergo further reduction

The i_d/i_r relation for this scheme has been derived by the author's previous unpublished work with Dr. Halina Wroblowa at the University of Pennsylvania, as:

$$\frac{i_d}{i_r} = \frac{1}{N}\left\{1 + \frac{2K1}{K_2} + A + \frac{K_6}{Z\sqrt{\omega}}\ A\right\}$$

$$A = \frac{2K1}{K_2K_5}(K_2 + K_3 + K_4) + \frac{2K3 + K_4}{K_5}, \quad Z = 0.62\ D^{2/3}\ \nu^{-1/6}$$

where N is the collecting efficiency of the ring, D is the diffusion coefficient, and ν the kinematic viscosity.

One typical example of this plot is shown on Figure 15 for 0.1 N KOH electrolyte at 25°C. The plot of i_d/i_r versus $1/\sqrt{\omega}$, at the disk potential up to -600 mv SCE, has an intercept close to 3.0 and a slope of zero at an extrapolated infinite rotating speed. It may be worth while to note that 3.0 is the reciprocal of the collecting efficiency of the ring measured by the $Fe(CN)_6^{+3}$, $Fe(CN)_6^{+4}$ redox couple. By examining the Eq. (9), it is clearly indicated that the oxygen reduces only to H_2O_2 (HO_2^-) by a two-electron process, no further reduction taking place before -600 mv SCE. Further cathodical polarization causes the slopes to increase, and further reduction of $H_2O_2(HO_2^-)$ is indicated. However, the interception still remains the same. By analyzing Eq. (9), it is indicated that K_5 and K_6 must be relatively large and $(2K_3 + K_4)$ has a finite value. The possibility of having four-electron reduction from O_2 to OH^- directly is small, in other words K_1 is negligible compared to K_2. At this stage, no clear distinction can be made between K_3 and K_4 by our results. However, the potential dependence tends to reveal that the existence of K_3 is more favorable than K_4.

The i_d/i_r analysis obtained for all the KOH electrolytes meet this description, except in the maximum peak region for the polarization curves obtained in 0.5N and some 1N KOH concentrations. The i_d/i_r plots are unrealiable for quantitative analysis because of the lack of reproducibility of these maximum peaks. A set of separate studies were made by setting the disk potential at various potentials in the maximum peak region and then varying the rotating speed; the change in surface conditions can be minimized during the period of measurement at the potentials. And linear relationships of i_d/i_r vs $1/\sqrt{\omega}$ were obtained with various slopes intercepts close to 3.0 at various potentials. These results further confirmed our previous explanation that the maximum current is contributed by the further reduction of H_2O_2 following the path K_3 or K_4, and is not due to four-electron direct reduction of K_1.

FIGURE 15

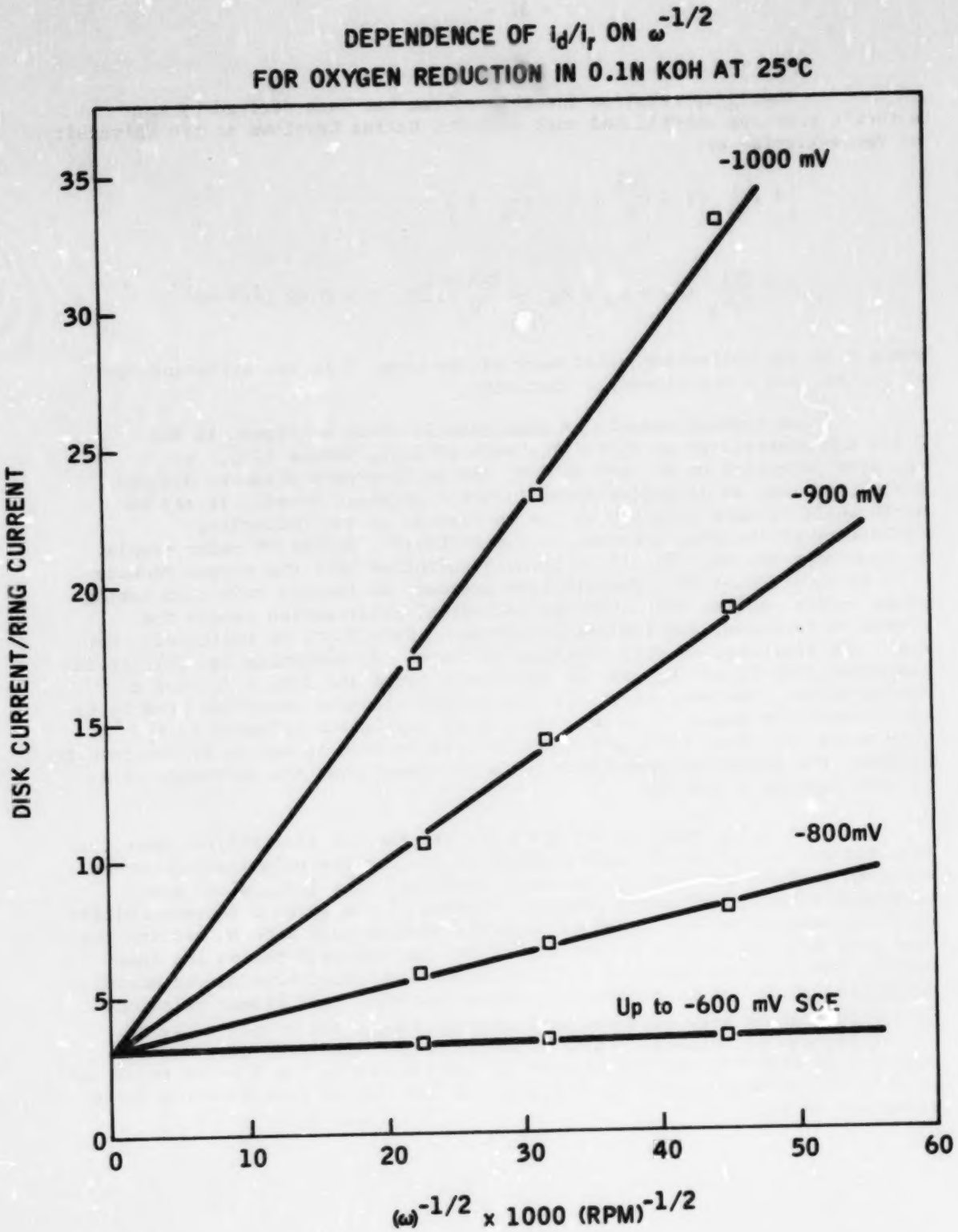
DEPENDENCE OF i_d/i_r ON $\omega^{-1/2}$
FOR OXYGEN REDUCTION IN 0.1N KOH AT 25°C
DISK CURRENT/RING CURRENT
$(\omega)^{-1/2}$ x 1000 $(RPM)^{-1/2}$
-1000 mV
-900 mV
-800mV
Up to -600 mV SCE
0
5
10
15
20
25
30
35
0
10
20
30
40
50
60

6.1.3 Diffusion Limited

The diffusion limiting currents for the two electron process,

$$O_2 + 2H^+ \xrightarrow{2e} H_2O_2 \ (HO_2^-) \qquad (10)$$

are reported in Table 3 for various KOH concentrations, temperatures and rotating speeds.

The theoretical limiting current can be expressed as (11):

$$i_L = 2FC_{bulk}\,\omega^{\frac{1}{2}}\,\nu^{\frac{1}{6}}\left(\frac{0.6205\ Sc^{-2/3}}{1 + 0.298\ Sc^{-1/3} + 0.14514\ Sc^{-2/3}}\right) \qquad (11)$$

where i_L is the diffusion limiting current in A/cm^2, F the Faraday constant in coulomb, C_{bulk} the bulk concentration in $mole/cm^3$, ω the angular velocity in rad/sec, ν the kinematic viscosity in cm^2/sec, D the diffusion coefficient in cm^2/sec, and Sc the Schmidt number (ν/D). The limiting currents were plotted versus $\omega^{\frac{1}{2}}$ and the necessary linear relationship was obtained in each case. The plots are shown in Figures 16-18. The slope of these plots contain information of the solubility and the diffusion coefficient of oxygen in various electrolytes.

6.1.4 Double Layer Capacitance and Residual Current

The double layer capacitance of the graphite electrode was measured, as described in the Experimental section, by the transient charging curves. The capacitance measured in 0.1 N KOH increased slowly from 4.6 μF to 40 μF during a period of two weeks and then remained constant. We believe that this is due to the electrolyte wetting the pores of the graphite.

The residual currents measured in N_2 were neglegible compared to the current of the polarization curves over the entire potential range. The residual currents in the operating range of air or oxygen cells, 1.0-0.6 V (FHE), are generally in the order of a tenth of μA. The oxidation current of the carbon is one of the contributors to these residual currents; based on the magnitude of the observed residual currents, the level of oxidation of carbon in KOH is not significant.

Table 3

Limiting Current For $O_2 + H^+ \xrightarrow{2e} H_2O_2(HO_2^-)$, (mA/cm^2)

	25°C	50°C	75°C	ω(rpm)
4N KOH	.21	.28	.27	500
	.29	.41	.38	1000
	.43	.60	.50	2000
2N KOH	0.57	.65	.63	500
	0.82	.96	.87	1000
	1.15	1.34	1.23	2000
1N KOH	.96	1.03	.90	500
	1.34	1.45	1.28	1000
	1.89	2.02	1.79	2000
0.5N KOH	1.24	1.36	1.31	500
	1.75	1.91	1.79	1000
	2.51	2.77	2.45	2000
0.1N KOH	1.26	1.34	1.42	500
	1.78	1.91	2.02	1000
	2.46	2.68	2.73	2000

FIGURE 16

DEPENDENCE OF LIMITING CURRENT ON $\omega^{1/2}$ IN KOH SOLUTION AT 25°C

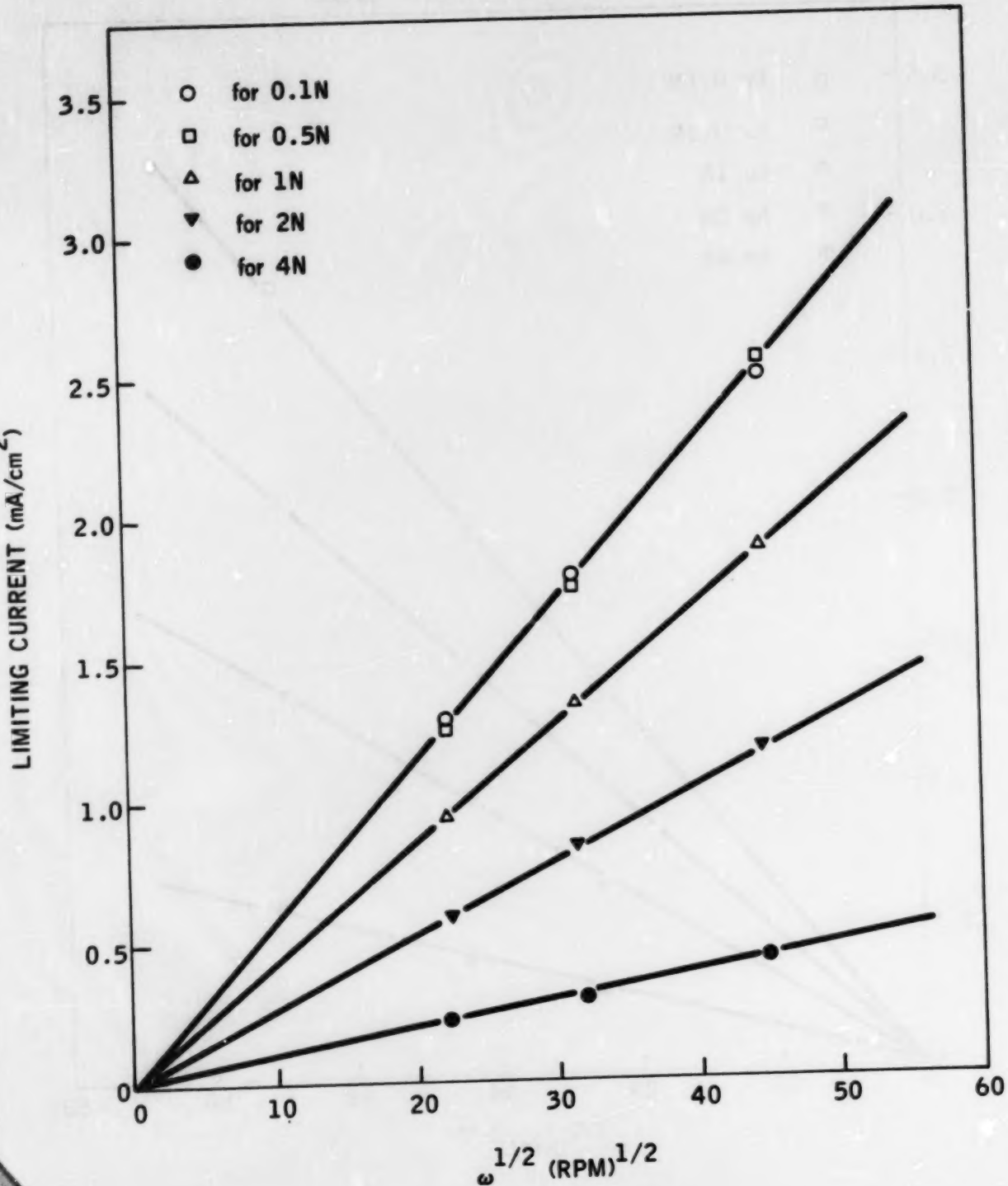

FIGURE 17

DEPENDENCE OF LIMITING CURRENT ON $\omega^{1/2}$ IN KOH SOLUTION AT 50°C

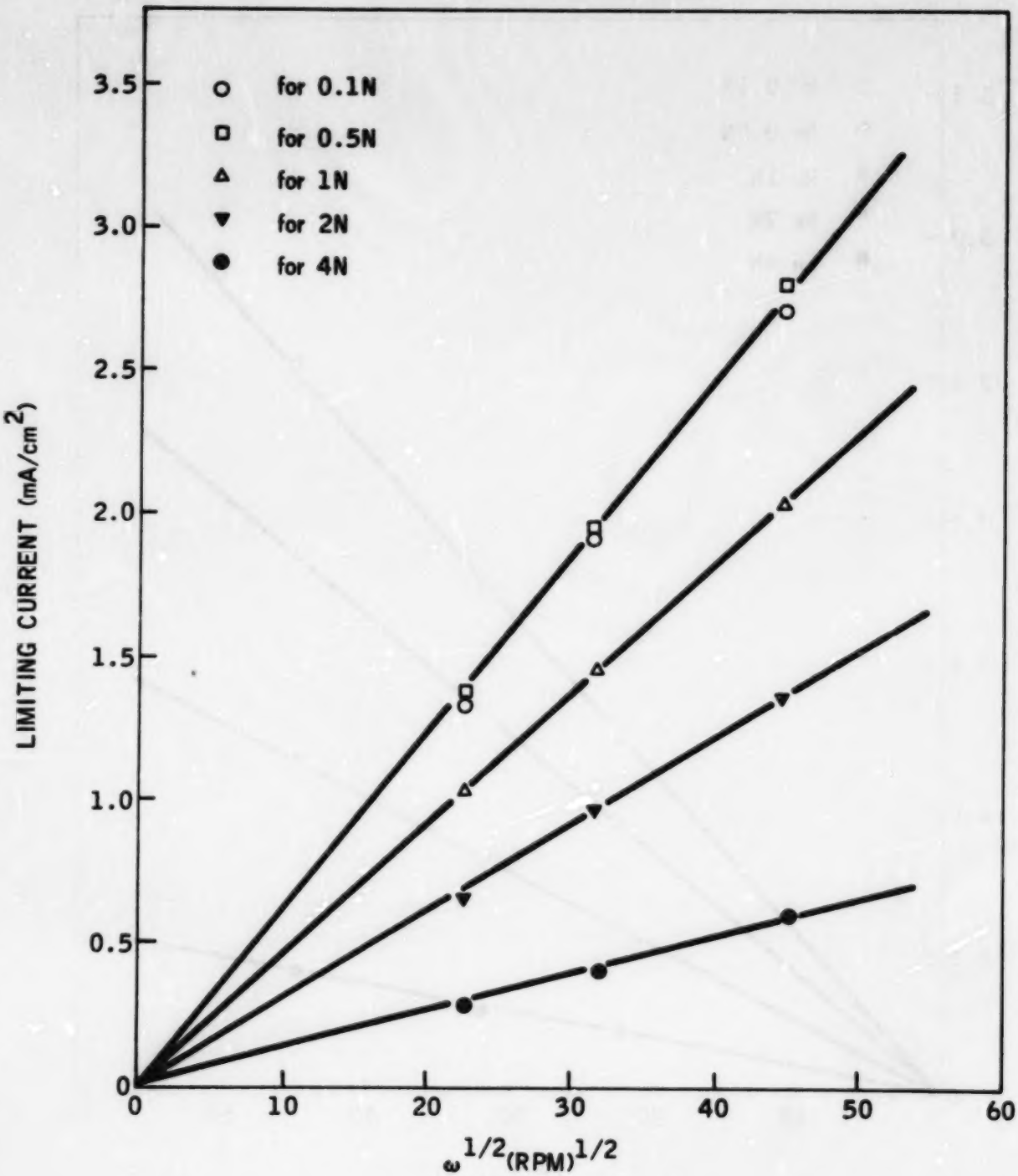

FIGURE 18

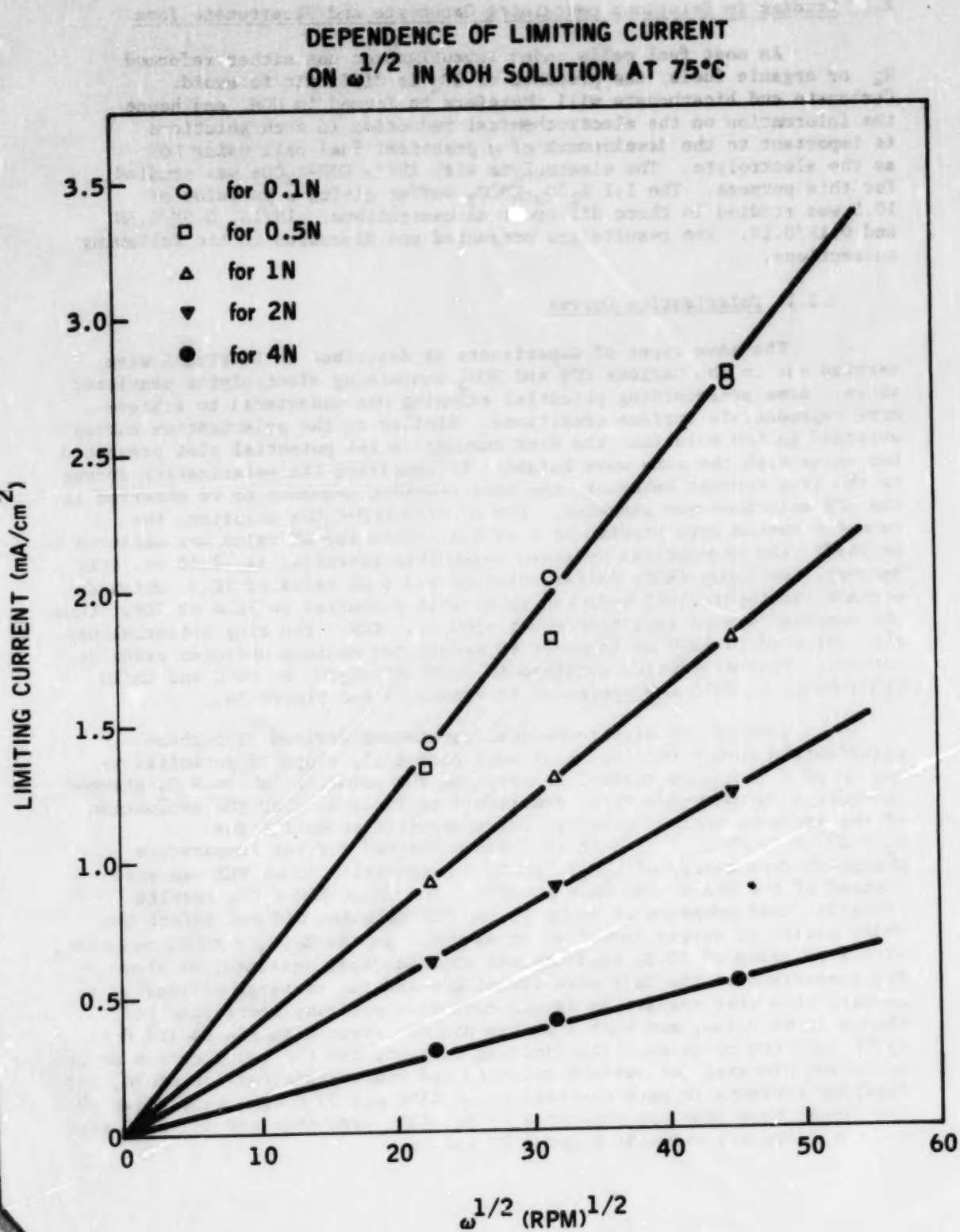
DEPENDENCE OF LIMITING CURRENT ON $\omega^{1/2}$ IN KOH SOLUTION AT 75°C
for 0.1N
for 0.5N
for 1N
for 2N
for 4N
LIMITING CURRENT (mA/cm^2)
$\omega^{1/2}$ (RPM)$^{1/2}$
0
0.5
1.0
1.5
2.0
2.5
3.0
3.5
0
10
20
30
40
50
60

6.2 Studies in Solutions containing Carbonate and Bicarbonate Ions

As most fuel cells under investigation use either reformed H_2 or organic fuels, the presence of CO_2 is difficult to avoid. Carbonate and bicarbonate will therefore be formed in KOH, and hence the information on the electrochemical reduction in such solutions is important to the development of a practical fuel cell using KOH as the electrolyte. The electrolyte with 2N/1M KOH-K_2CO_3 was studied for this purpose. The 1:1 K_2CO_3-$KHCO_3$ buffer giving a pH value of 10.3 was studied in three different concentrations: 1N/1N, 0.5N/0.5N and 0.1N/0.1N. The results are presented and discussed in the following subsections.

6.2.1 Polarization Curves

The same types of experiments as described in Section 5 were carried out in the various $CO_3^=$ and HCO_3^- containing electrolytes mentioned above. Same prerecording potential scanning was undertaken to achieve more reproducible surface conditions. Similar to the polarization curves obtained in KOH solution, the disk current vs its potential plot presented two waves with the same wave height. By comparing the polarization curves to the ring current behavior, the same reaction sequence as we observed in the KOH solutions was expected. For a 2N/1M KOH-K_2CO_3 solution, the recorded sweeps were started at 0 mV SCE, since the pH value was measured to be 14.59 (the theoretical hydrogen reversible potential is -1.10 vs. SCE). However, the K_2CO_3-$KHCO_3$ buffer solution has a pH value of 10.3, which decreases the theoretical hydrogen reversible potential to -850 mV SCE. Thus, the recorded sweeps were started at +100 mV. SCE. The ring potential was also adjusted to +350 mV in order to detect the maximum hydrogen peroxide current. Typical results obtained in 2N/1M KOH-K_2CO_3 at 50°C and 1M/1M K_2CO_3-$KHCO_3$ at 75°C are presented in Figure 19 and Figure 20.

Some of the electrochemical parameters derived from these polarization curves such as, half-wave potential, slope of potential vs log i_a plot, exchange current density and the potential where H_2O_2 started to undergo further reduction, are listed in Table 4. For the evaluation of the exchange current density, the reversible potential for $O_2 + 2H^+ + 2e \rightleftharpoons H_2O_2$ at 75°C was corrected for the temperature change of free energy of H_2O_2: at 75°C potential 633 mV RHE was used instead of the 682 mV RHE used at 25°C. The 2N/1M KOH-K_2CO_3 results indicate that presence of K_2CO_3 in the KOH solution did not affect the polarization of oxygen reduction on carbon. In the K_2CO_3 + $KHCO_3$ solution, with a pH value of 10.3, activity was significantly lessened, as shown by the comparison of the half wave potentials and the exchange currents. It appears then that changes in oxygen reduction activity correspond to change in pH value, and such a change did not occur with the addition of K_2CO_3 into KOH solution. The limiting currents for the two electron oxygen reduction process, for various solution and temperature were obtained, and limiting currents in each electrolyte at 25°C and 75°C were plotted vs $\omega^{\frac{1}{2}}$. The linear relationships predicted by Eq. (11) were obtained in both cases, and the plots are shown in Figures 21 and 22.

FIGURE 19

REDUCTION OF OXYGEN ON GRAPHITE IN 2N/1M KOH-K_2CO_3 AT 50°C

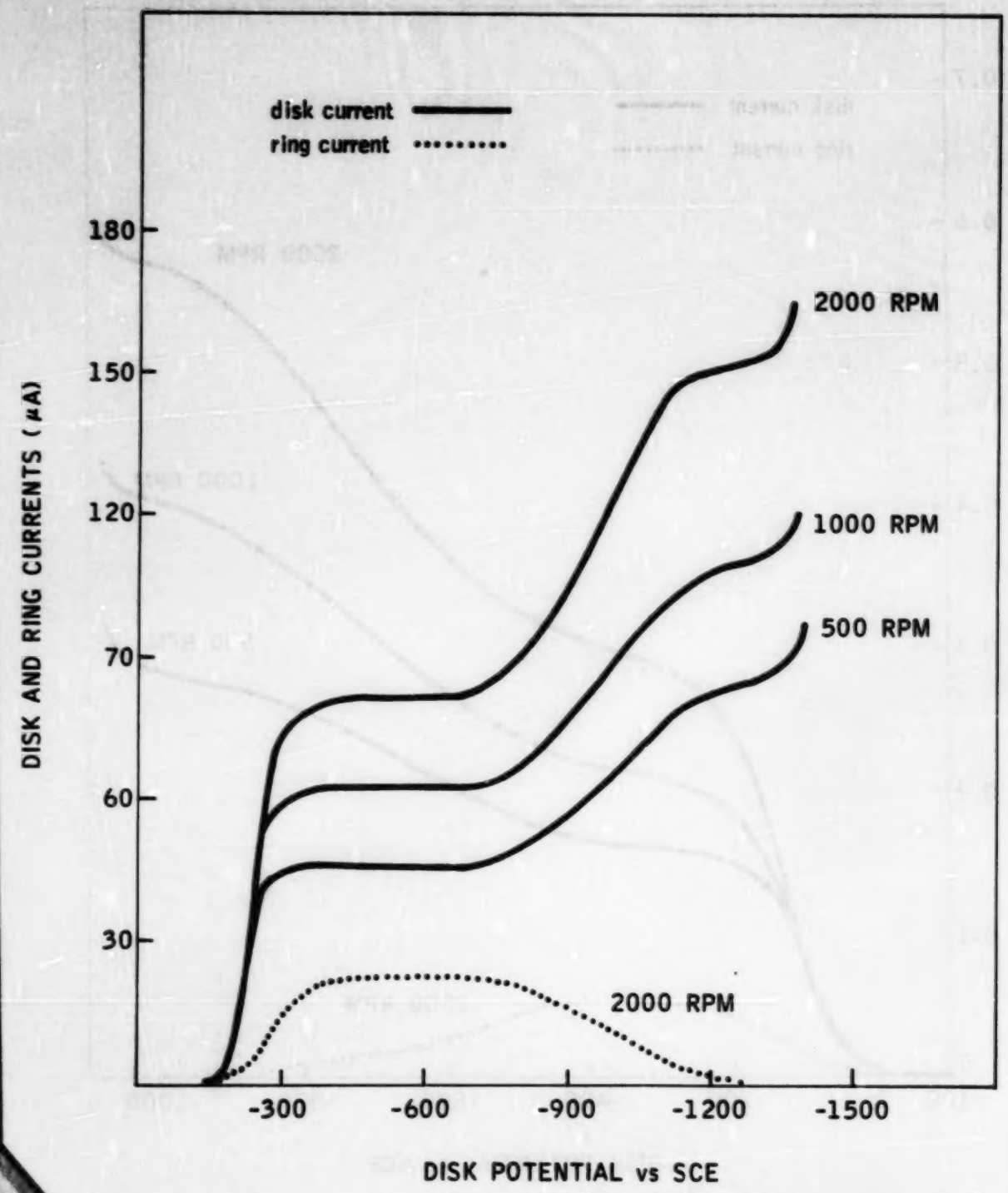

FIGURE 20

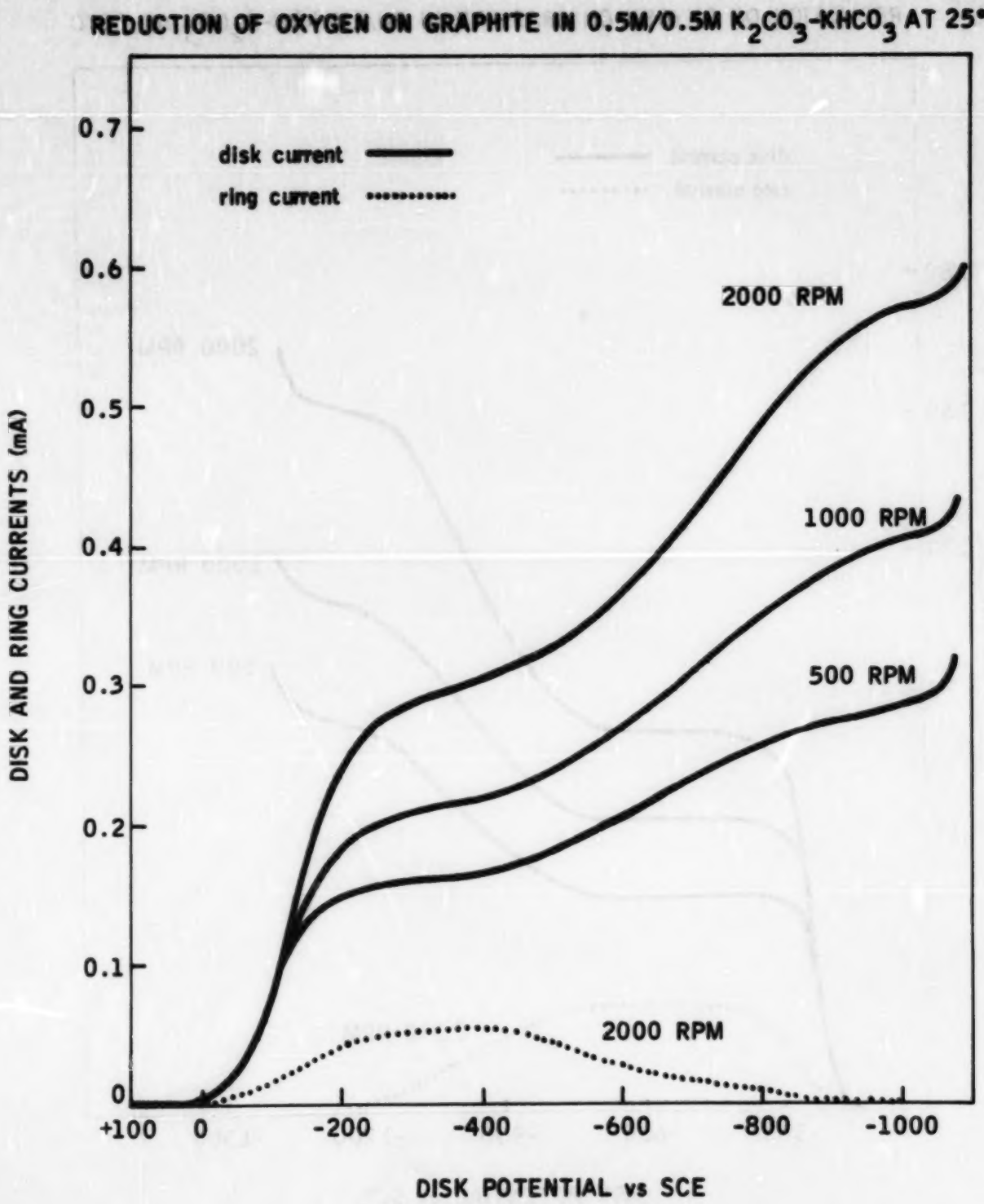
REDUCTION OF OXYGEN ON GRAPHITE IN 0.5M/0.5M K_2CO_3-$KHCO_3$ AT 25°C
disk current
ring current
2000 RPM
1000 RPM
500 RPM
2000 RPM
0.7
0.6
0.5
0.4
0.3
0.2
0.1
0
+100
0
-200
-400
-600
-800
-1000
DISK AND RING CURRENTS (mA)
DISK POTENTIAL vs SCE

Table 4

Parameters Involved in the Determination of the Oxygen Reduction Reaction Activity in Solutions Containing Carbonate and Bicarbonate Ions

Concentration and Composition	Temperature °C	Slope of Potential vs log i_a plot (mV/decade)	$E_{\frac{1}{2}}$ (mV vs SCE)	$E_{\frac{1}{2}}$ (mV vs RHE) (a)	io (A/cm^2) (b)	$E_{H_2O_2}$ (mV vs SCE) (c)
2N/ 1M $KOH-K_2CO_3$ (pH=14.57)	75°C	78	-205	895	4×10^{-2}	-600
	50°C	78	-223	877	3×10^{-2}	-750
	25°C	79	-216	884	2×10^{-2}	-760
1M/1M K_2CO_3 - $KHCO_3$ (pH=10.3)	75°C	72	-99	751	3×10^{-2}	-400
	25°C	100	-134	716	1×10^{-3}	-400
0.5M/0.5M K_2CO_3-$KHCO_3$ (pH=10.3)	75°C	59	-86	764	2×10^{-2}	-380
	25°C	81	-124	726	4×10^{-3}	-360
0.1M/0.1M K_2CO_3-$KHCO_3$ (pH=10.3)	75°C	92	-128	722	1×10^{-2}	-380
	25°C	125	-173	677	2×10^{-3}	-400

(a) $E_{\frac{1}{2}}$, half wave potential
(b) io, the exchange current density
(c) $E_{H_2O_2}$, the potential where H_2O_2 starts to undergo further reduction

FIGURE 21

DEPENDENCE OF LIMITING CURRENT ON $\omega^{1/2}$ IN SOLUTIONS CONTAINING CARBONATE AND BICARBONATE AT 25°C

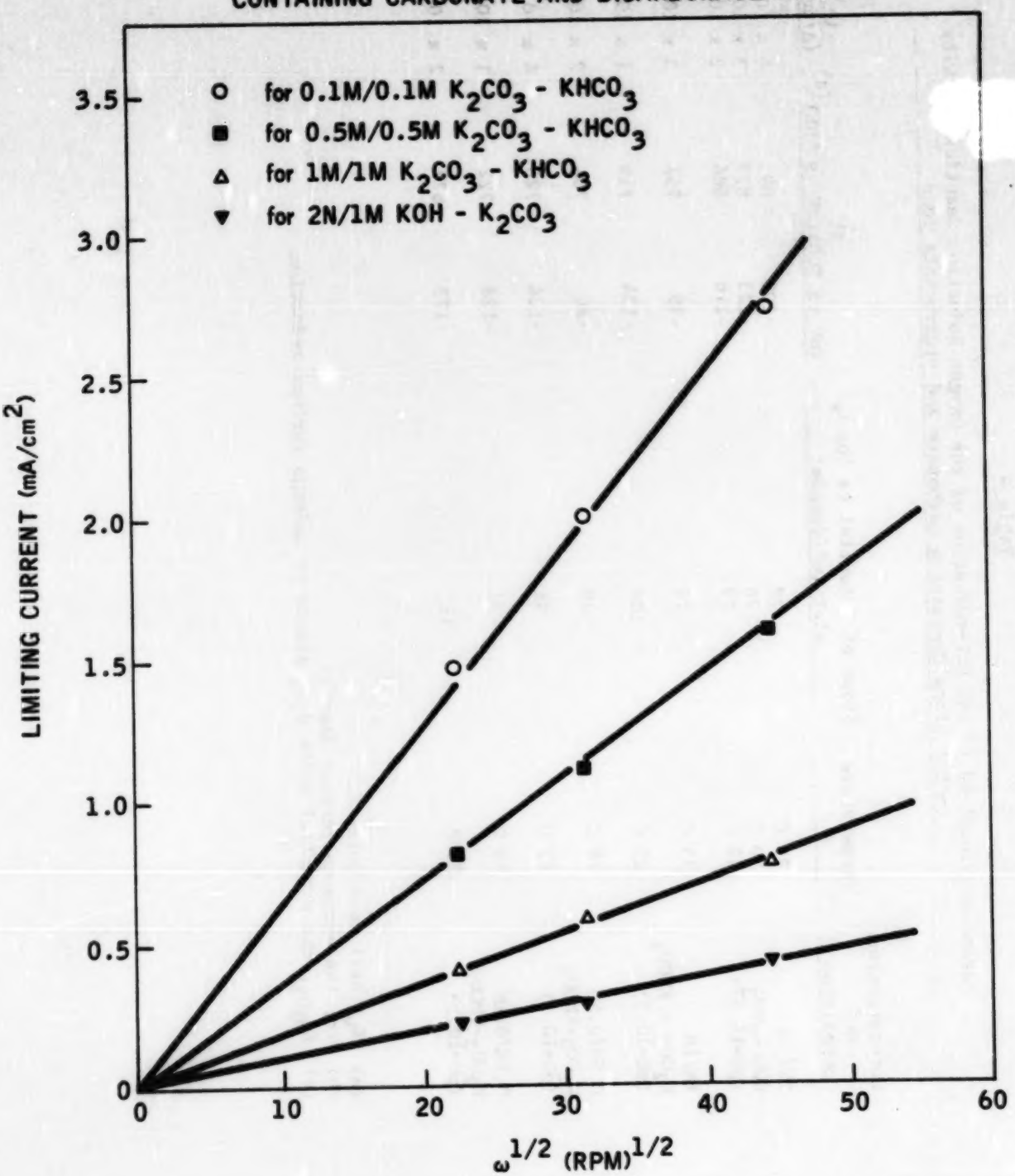

FIGURE 22

DEPENDENCE OF LIMITING CURRENT ON $\omega^{1/2}$ IN SOLUTIONS CONTAINING CARBONATE AND BICARBONATE AT 75°C

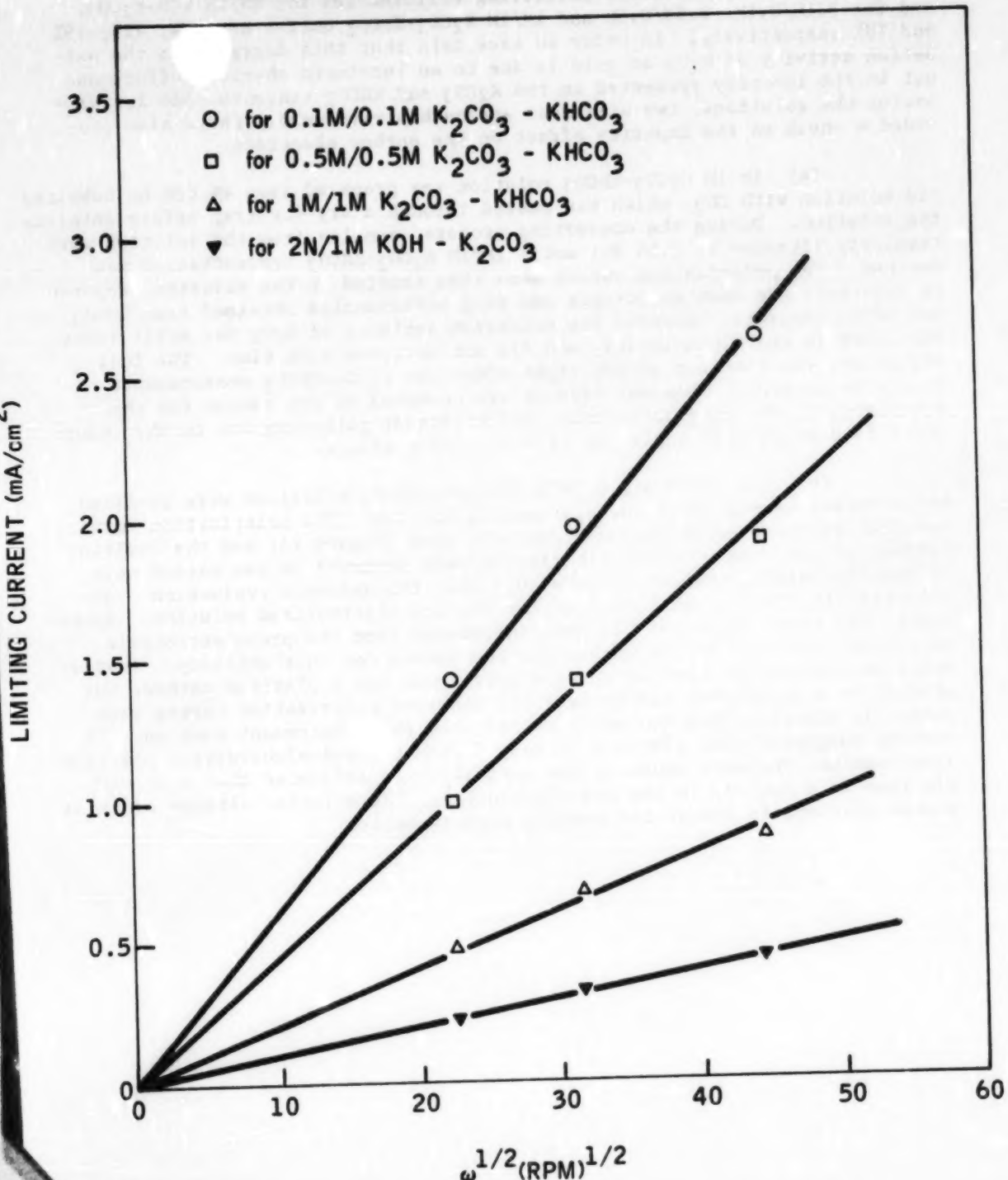

6.2.2 The Effect of Impurities

The $CO_3^=$ and HCO_3^- containing electrolyte, the collecting efficiency of the ring decreased with decreasing of pH values and also with increasing concentration of $CO_3^=$ and HCO_3^-. The reproducibility of the ring current also decreased. The approximated collecting efficiencies for 2N/2N KOH-K_2CO_3, and for 0.1M/0.1M, 0.5M/0.5M and 1M/1M K_2CO_3-$KHCO_3$ buffer are 27%, 22%, 19% and 18% respectively. In order to ascertain that this decrease in the oxidation activity of H_2O_2 on gold is due to an intrinsic chemical effect and not to the impurity presented in the K_2CO_3 and $KHCO_3$ reagents used for preparing the solutions, two different approaches were used. These also provided a check on the impurity effect on the carbon electrode.

(a) 1M/1M K_2CO_3-$KHCO_3$ solution was prepared from 4N KOH by bubbling the solution with CO_2, which was passed through a dry ice trap before entering the solution. During the converting process, samples from the solution were regularly titrated by 0.1N HCl until 1M/1M K_2CO_3-$KHCO_3$ concentration was reached. The polarization curves were then studied in the solution prepared in this way; the disk activities and ring efficiencies obtained from K_2CO_3 and $KHCO_3$ reagents. However the oxidation activity of H_2O_2 was still lower than that in the KOH solution, and did not decrease with time. The full efficiency was restored in KOH right after the K_2CO_3-$KHCO_3$ measurements. Therefore intrinsic chemical effects are accepted as the reason for the decreasing of the ring activities, and electrode poisoning due to the impurities is considerably small, or is a secondary effect.

(b) The 1M/1M and 0.5M/0.5M K_2CO_3-$KHCO_3$ solutions were purified by pre-electrolysis using two platinum electrodes. The polarization curves obtained in these solutions have only one wave (Figure 23) and the limiting current is comparable to the limiting current observed in the second wave of normally used solutions (Figure 20); also the hydrogen evoluation overpotential is significantly reduced for the pre-electrolized solution. Apparently, the trace amount of platinum introduced from the pre-electrolysis electrode deposited on the carbon was the reason for this activity. Another solution pre-electrolized by using a gold anode and a platinum cathode was studied on a repolished electrode. The observed polarization curves were gradually changing from two waves to one when the measurement went on. It further suggested that platinum dissolved from the pre-electrolysis platinum electrode was the main cause of the activity. It indicated that even with platinum as a cathode in the pre-electrolysis, the solution already contains enough platinum to change the results significantly.

FIGURE 23

REDUCTION OF OXYGEN ON GRAPHITE IN
PREELECTROLIZED 0.5M/0.5M K_2CO_3-$KHCO_3$ AT 25°C

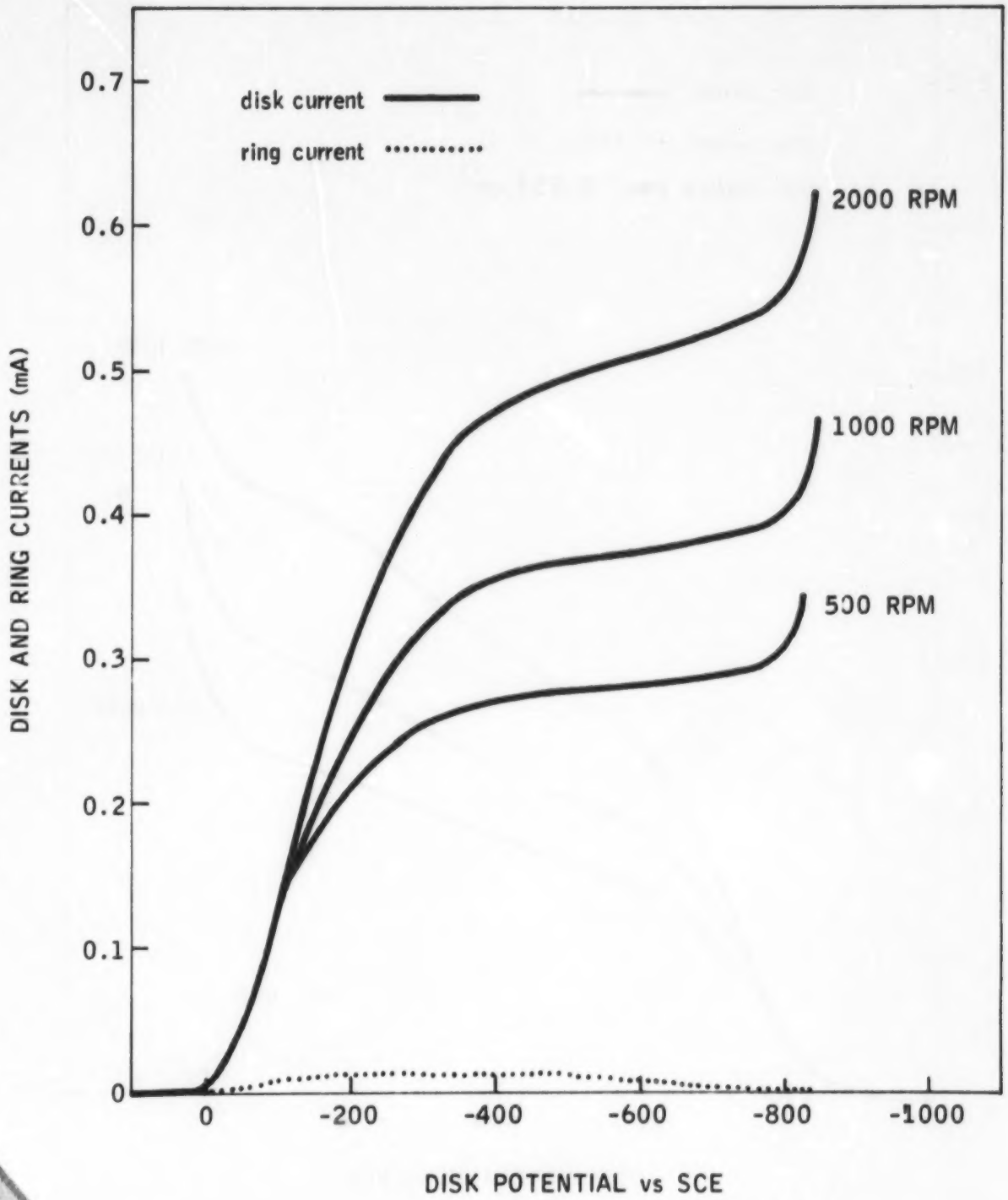

FIGURE 24

REDUCTION OF OXYGEN ON GRAPHITE IN 1M/1M KH_2PO_4 - K_2HPO_4 AT 75°C

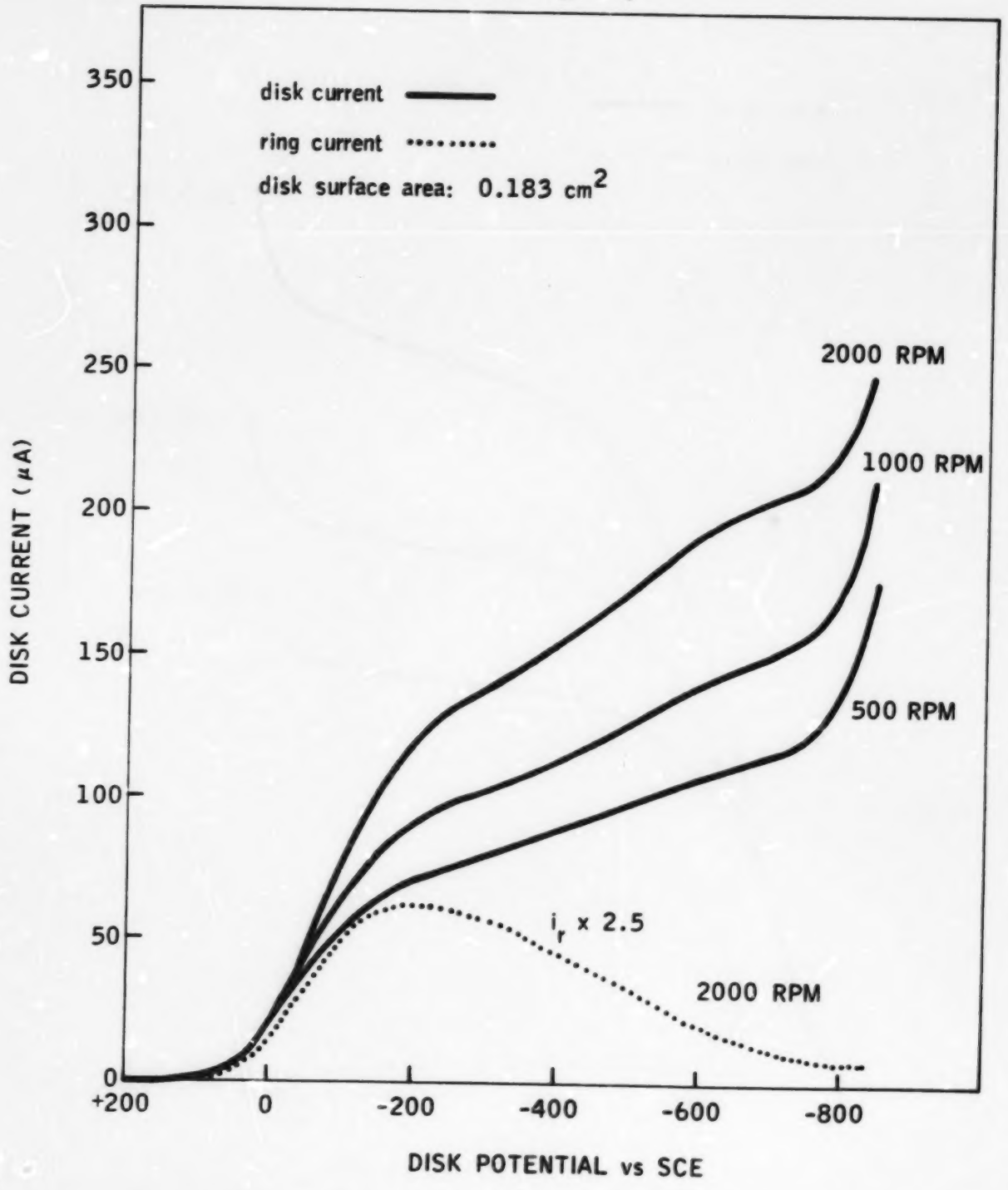

FIGURE 25

REDUCTION OF OXYGEN ON GRAPHITE IN 1M/1M
KAcO - HAcO AT 75°C

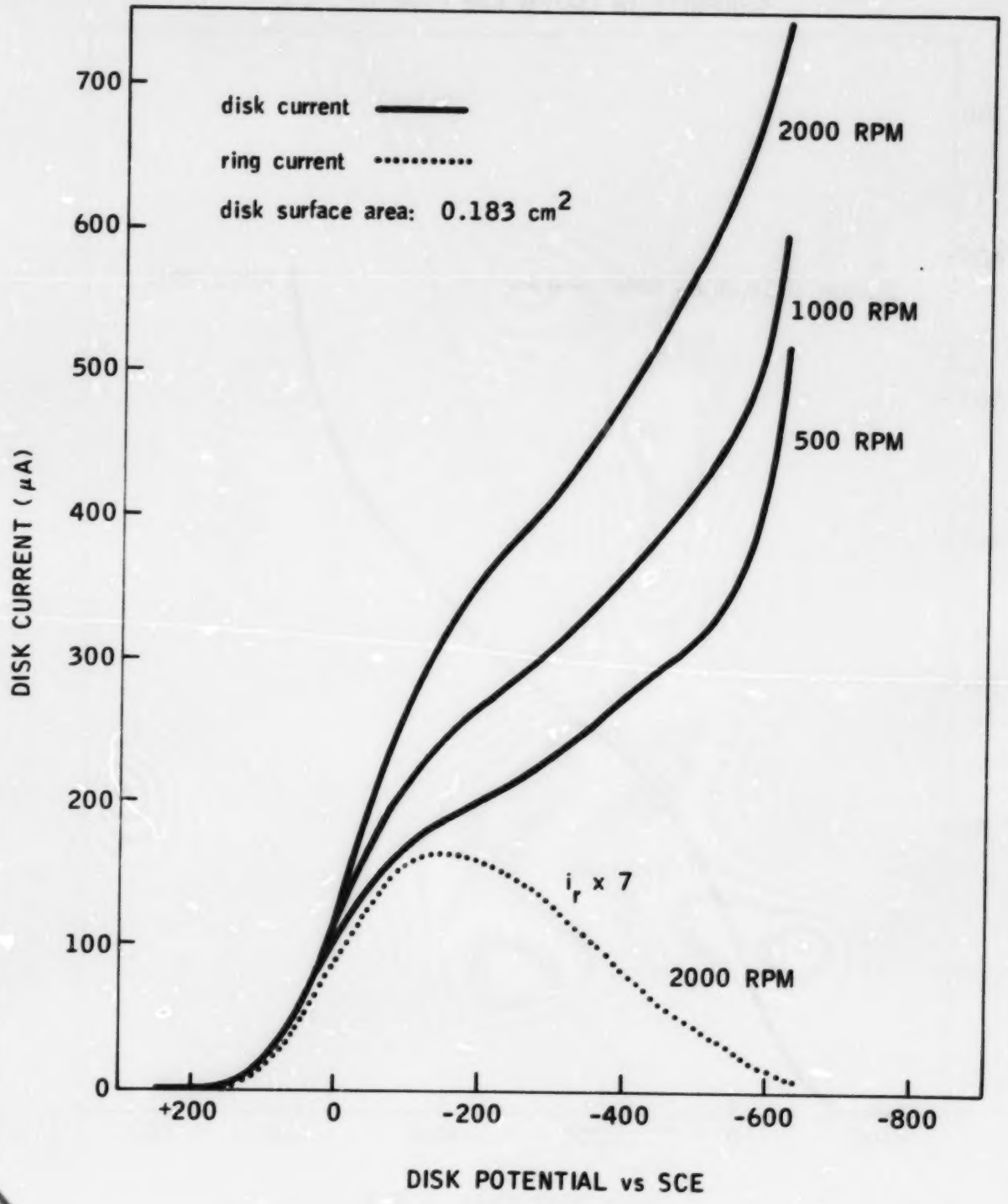

FIGURE 26

REDUCTION OF OXYGEN AND HYDROGEN PEROXIDE ON GRAPHITE IN 1M/1M KAc - HAc AT 75°C

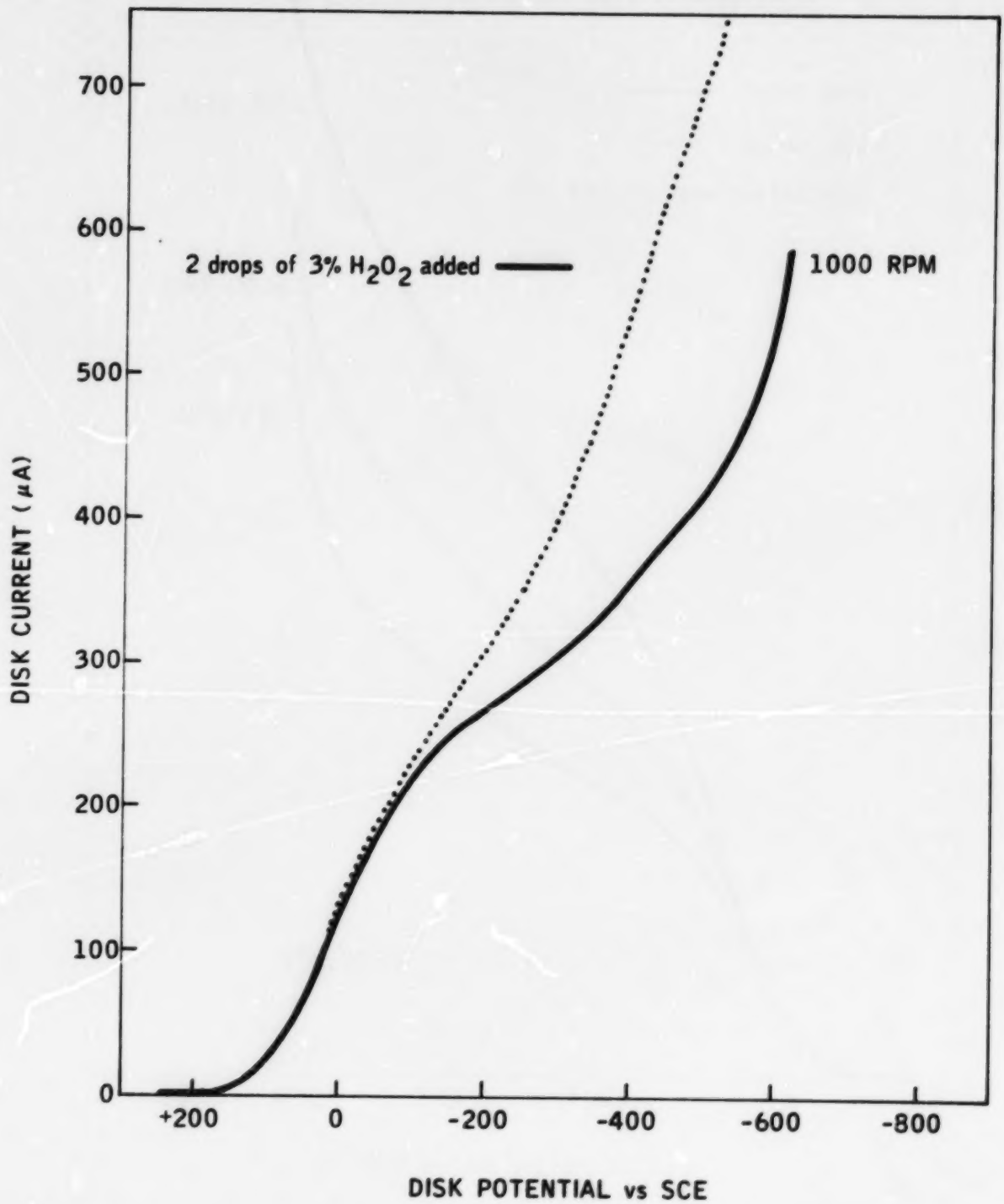

Table 5

Parameters Involved in the Determination of the Oxygen Reduction Reaction Activity in Buffer Solutions Containing Phosphate

Concentration and Composition	Temperature °C	Slop of Potential vs log ia plot (mV/decade)	$E_{\frac{1}{2}}$ (mV vs SCE)	$E_{\frac{1}{2}}$ (mV vs RHE)[a]	io (A/cm^2)[b]	$E_{H_2O_2}$ (mV vs SCE)[c]
1M/1M K_2HPO_4-KH_2PO_4 (pH=6.8)	75°C	108	-59	584	1.6×10^{-4}	-250
	25°C	99	-87	556	2×10^{-5}	-250
0.5M/0.5M K_2HPO_4-KH_2PO_4 (pH=6.8)	75°C	105	-83	560	2×10^{-4}	-240
	25°C	136	-135	508	4×10^{-5}	-360
0.1M/0.1M K_2HPO_4-KH_2PO_4 (pH=6.8)	75°C	100	-107	536	2×10^{-4}	-230
	25°C	128	-140	503	6×10^{-5}	-350
1M/1M H_3PO_4-KH_2PO_4 (pH=2.1)	75°C	140	+75	440	5×10^{-5}	beyond hydrogen evolution
	25°C	140	+10	375	7×10^{-6}	beyond hydrogen evolution
0.1M/0.1M H_3PO_4-KH_2PO_4 (pH=2.1)	75°C	154	+12	377	3×10^{-5}	-300
	25°C	159	-69	296	8×10^{-6}	beyond hydrogen evolution

(a) $E_{\frac{1}{2}}$, half wave potential
(b) id, the exchange current density
(c) $E_{H_2O_2}$, the potential where H_2O_2 starts to undergo further reduction

Table 6

Parameter Involved in the Determination of the Oxygen Reduction Reaction Activity in Potassium Acetate-Acetic Acid Buffers and Sulfuric Acid

Concentration and Composition	Temperature °C	Tafel Slope (mV/decade)	$E_{\frac{1}{2}}$ (mV vs SCE)	$E_{\frac{1}{2}}$ (mV vs RHE)[a]	io (A/cm^2)[b]	$E_{H_2O_2}$ (mV vs SCE)[c]
1M/1M KAcO -HAcO (pH=4.6)	75°C	125	-11	502	1×10^{-4}	-180
	25°C	125	-57	456	1.5×10^{-5}	-250
0.1M/0.1M KAcO -HAcO (pH=4.6)	75°C	135	-57	456	6×10^{-5}	-200
	25°C	175	-180	333	1.4×10^{-5}	-350
1N H_2SO_4 (pH=1)	75°C	115	+115	415	1.8×10^{-5}	beyond hydrogen evolution
	25°C	115	+23	323	1.1×10^{-6}	beyond hydrogen evolution

(a) $E_{\frac{1}{2}}$, half wave potential
(b) io, the exchange current density
(c) $E_{H_2O_2}$, the potential where H_2O_2 starts to undergo further reduction

FIGURE 27

DEPENDENCE OF LIMITING CURRENT ON $\omega^{1/2}$
IN SOLUTIONS CONTAINING PHOSPHATE AT 25°C

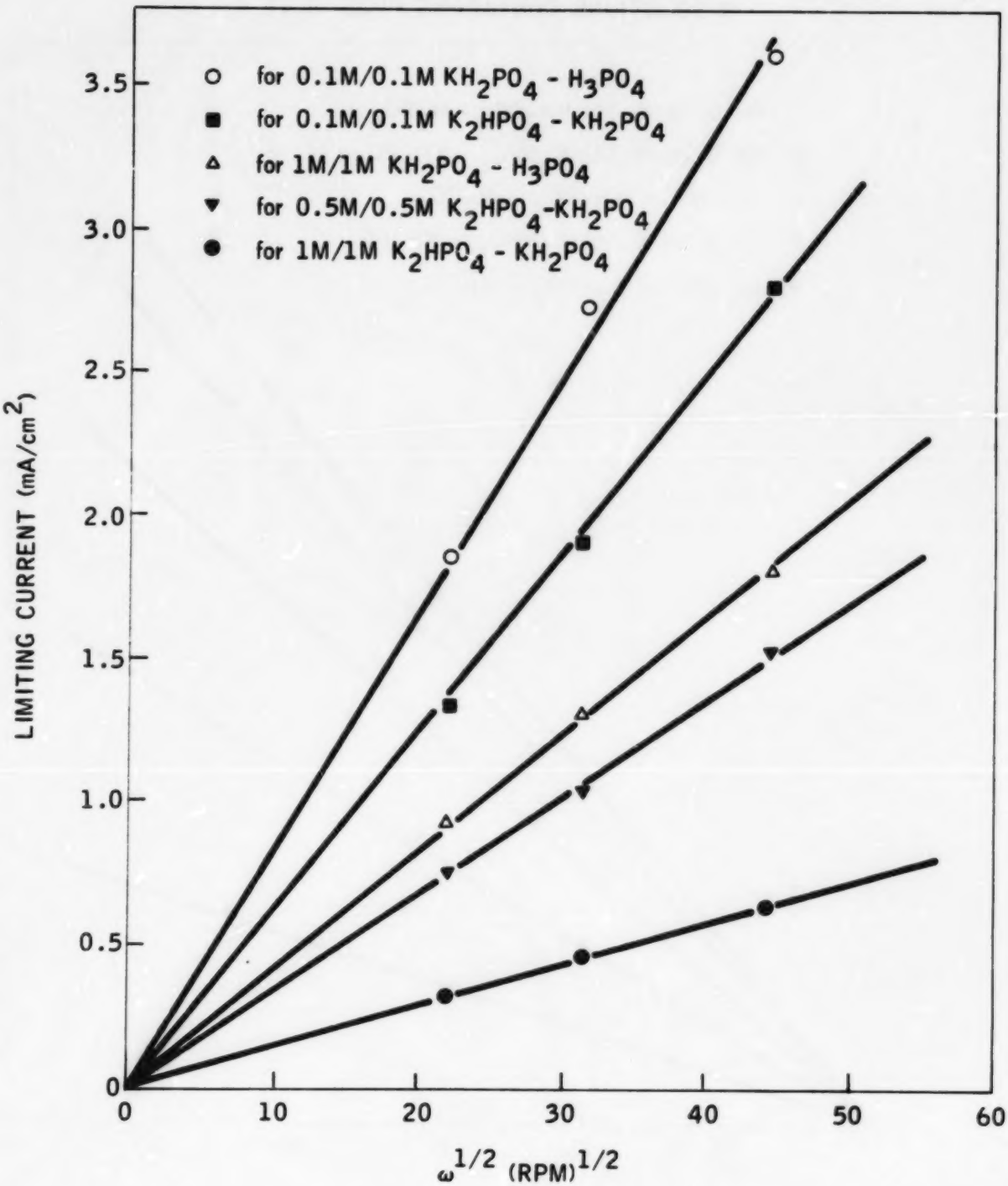

FIGURE 28

DEPENDENCE OF LIMITING CURRENT ON $\omega^{1/2}$
IN SOLUTIONS CONTAINING PHOSPHATE AT 75°C

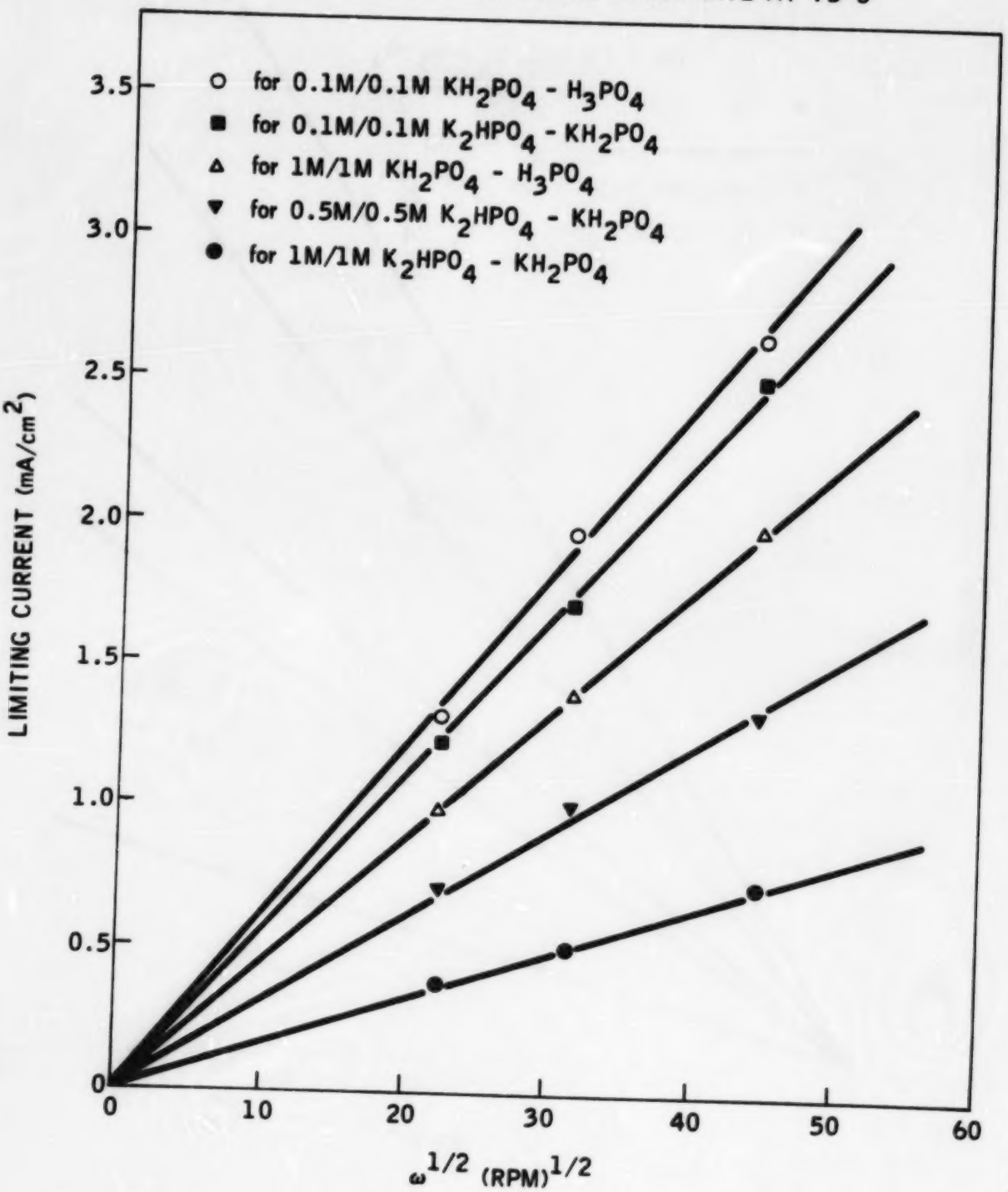

6.4 Studies in the Potassium Phosphate - Phosphoric Acid Buffer Solution and Sulfuric Acid

In order to investigate the pH dependence of the electrochemical reduction of oxygen on carbon, three solutions were studied: 1M/1M and 0.1M/0.1M KH_2PO_4-H_3PO_4 with a pH value of 2.1, and 0.1N H_2SO_4 with a pH value of 1. The polarization curves were studied at 25°C and 75°C.

The polarization curves in these solutions were studied following the procedure described in the experimental section. In 1:1 KH_2PO_4-H_3PO_4 buffers, the current was recorded starting at +400 mV SEC, and in the 0.1N H_2SO_4 solution it was recorded starting at +450 mV SEC, with ring potential of +1.35 V and +1.50 V SCE respectively to detect the hydrogen peroxide formed on the disk electrode. The rate of oxidation of H_2O_2 on the ring was very low in these solutions-the collection efficiency was approximated to be 5%. It varied with the concentration, lower collection efficiency being always associated with higher concentration.

The patterns of the polarization curves obtained from these solutions were also similar. Only one wave was observed (Figures 29 and 30). Examination of the shape of the ring current indicated that H_2O_2 was not being further reduced. It is assumed then that the reaction continued as a two-electron reduction process until hydrogen evolution potential. The hydrogen peroxide reduction process starts after the hydrogen evolution potential is covered by the overwhelming current from the hydrogen evolution; thus this hydrogen peroxide reduction current was not shown by a second wave, as it was in previous experiments. This assumption was confirmed by the response of the polarization curves when 2 drops of 3% H_2O_2 were added to the solution. The additional H_2O_2 in the solution did not increase the current (change the normally obtained curve) at 25°C: only a slight additional current was derived from these polarization curves, such as half-wave potential, Tafel slope and exchange current density are listed in Tables 5 and 6. The limiting current are approximated and plotted vs. $\omega^{1/2}$ for each concentration at two different temperatures are shown in Figure 31.

6.3 Studies in the Potassium Phosphate Buffer and the Potassium Acetate - Acetic Acid Buffer

The pH values of the 1:1 K_2HPO_4-KH_2PO_4 and the 1:1 KAcO-HAcO buffer solution are 6.8 and 4.6, respectively. In order to investigate the pH dependence and concentration effects of the electrochemical reduction of oxygen on carbon, five compositions were studied: 1M/1M, 0.5M/0.5M and 0.1M/0.1M of K_2HPO_4-KH_2PO_4 solution, and 1M/1M and 0.1M/0.1M of KAcO-HAcO solution. The polarization curves were studied at 25°C and 75°C.

The polarization curves for all the solutions described here were obtained by the procedures described in Section 5. In 1:1 K_2HPO_4-KH_2PO_4 buffers, the current was recorded from a disk potential of +200 MV SCE to the hydrogen evolution potential, with the ring potential set at +570 mV SCE. In 1:1 KAcO-HAcO buffers, recording was begun at a disk potential of +250 mV SCE and the ring potential was reset at +1.02 V SCE. The patterns of the polarization curves obtained for both buffers are similar, and are presented and discussed together below. In these solutions the waves representing the two separate oxygen reduction steps were more difficult to distinguish. Before the oxygen-reduction-to-hydrogen-peroxide wave reached the plateau, the hydrogen peroxide had already started to undergo further reduction, thus overlapping the first step of the reaction as shown in Figures 24 and 25. However, examination of the maximum at the ring current plot still enabled us to estimate with reasonable accuracy the limiting current of two-electron oxygen reduction and the potential where H_2O_2 reduction started taking place. After taking the normal polarization curves, two drops of 3% H_2O_2 were added to the solution to obtain another polarization curve. The results of the curves obtained (a) without and (b) with the addition of H_2O_2 were in agreement; ie at that potential where the ring current in (a) started to fall, the disk current in polarization curves (b) rapidly increased beyond values normally obtained without addition of H_2O_2 as shown in Figure 26.

Some of the electrochemical parameters derived from these polarization curves related to the oxygen reduction activities such as, half wave potential ($E_{\frac{1}{2}}$), Tafel slope, exchange current density and potential where H_2O_2 starts to undergo further reduction, are listed in Tables 5 and 6. To approximate the exchange current densitieis, the Tafel lines were extrapolated to the reversible potential of the $O_2 + 2H^+ \underset{}{\overset{2e}{\rightleftharpoons}} H_2O_2$ couple; the potential at 25°C is +682 mV RHE was used at 75°C. The limiting current plots vs $\omega^{\frac{1}{2}}$ for each electrolyte at two different temperatures are shown in Figures 27 and 28.

FIGURE 29

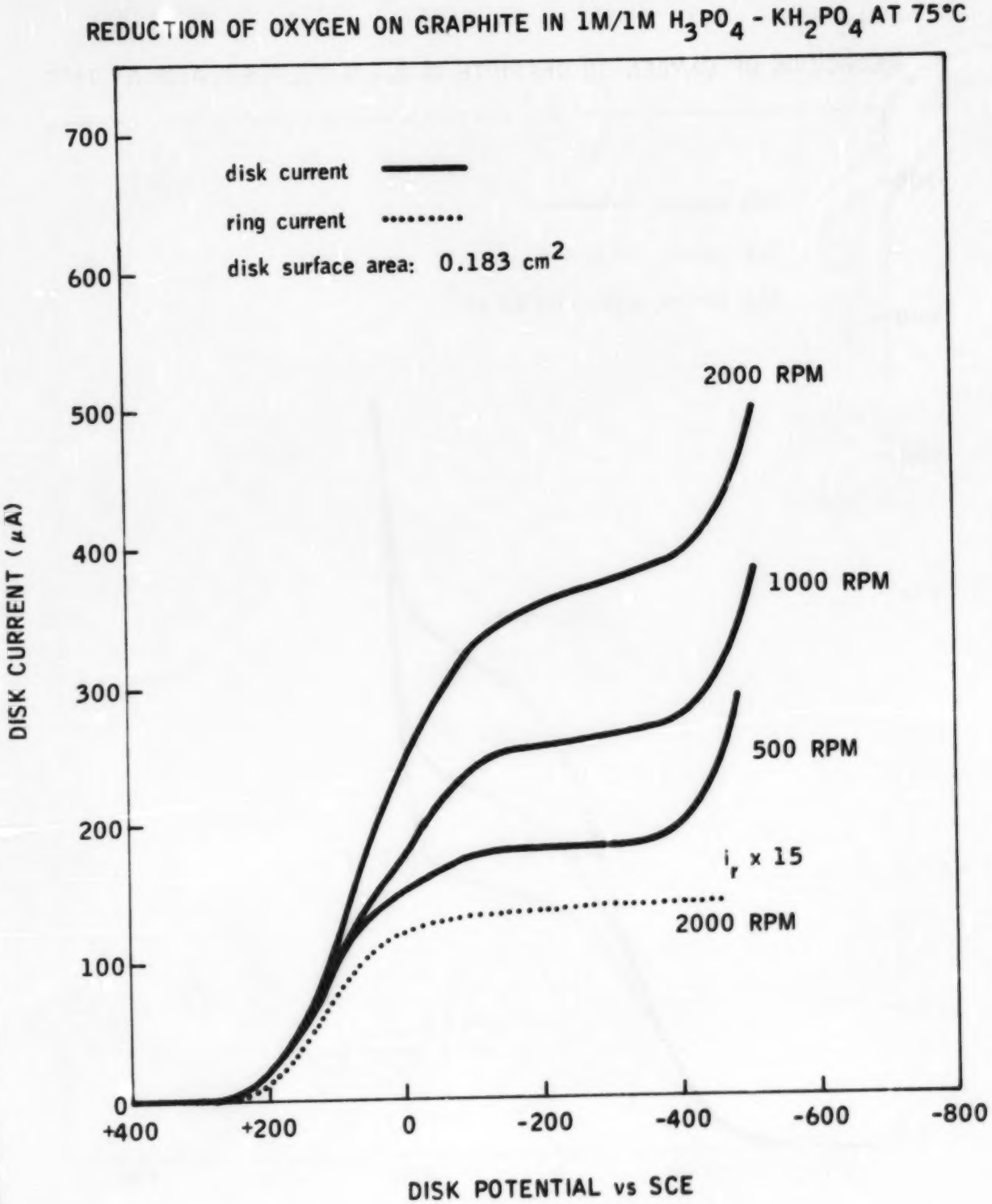
REDUCTION OF OXYGEN ON GRAPHITE IN 1M/1M H_3PO_4 - KH_2PO_4 AT 75°C
disk current
ring current
disk surface area: 0.183 cm^2
2000 RPM
1000 RPM
500 RPM
i_r x 15
2000 RPM
DISK CURRENT (μA)
700
600
500
400
300
200
100
0
+400
+200
0
-200
-400
-600
-800
DISK POTENTIAL vs SCE

FIGURE 30

REDUCTION OF OXYGEN ON GRAPHITE IN 0.1 N SULFURIC ACID AT 75°C

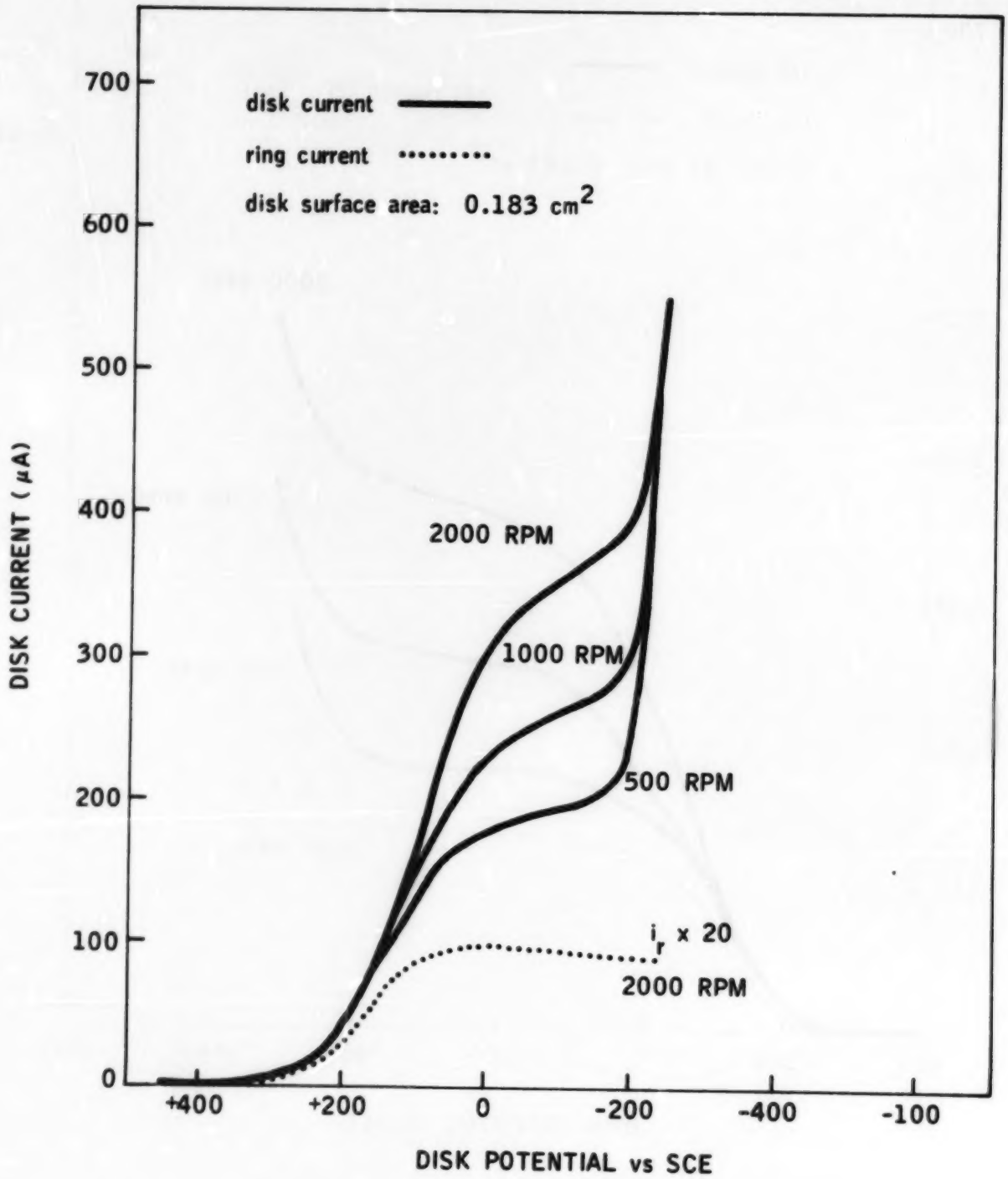

FIGURE 31

DEPENDENCE OF LIMITING CURRENT ON $\omega^{1/2}$ IN POTASSIUM ACETATE-ACETIC ACID BUFFER AND 0.1N SULFURIC ACID SOLUTION

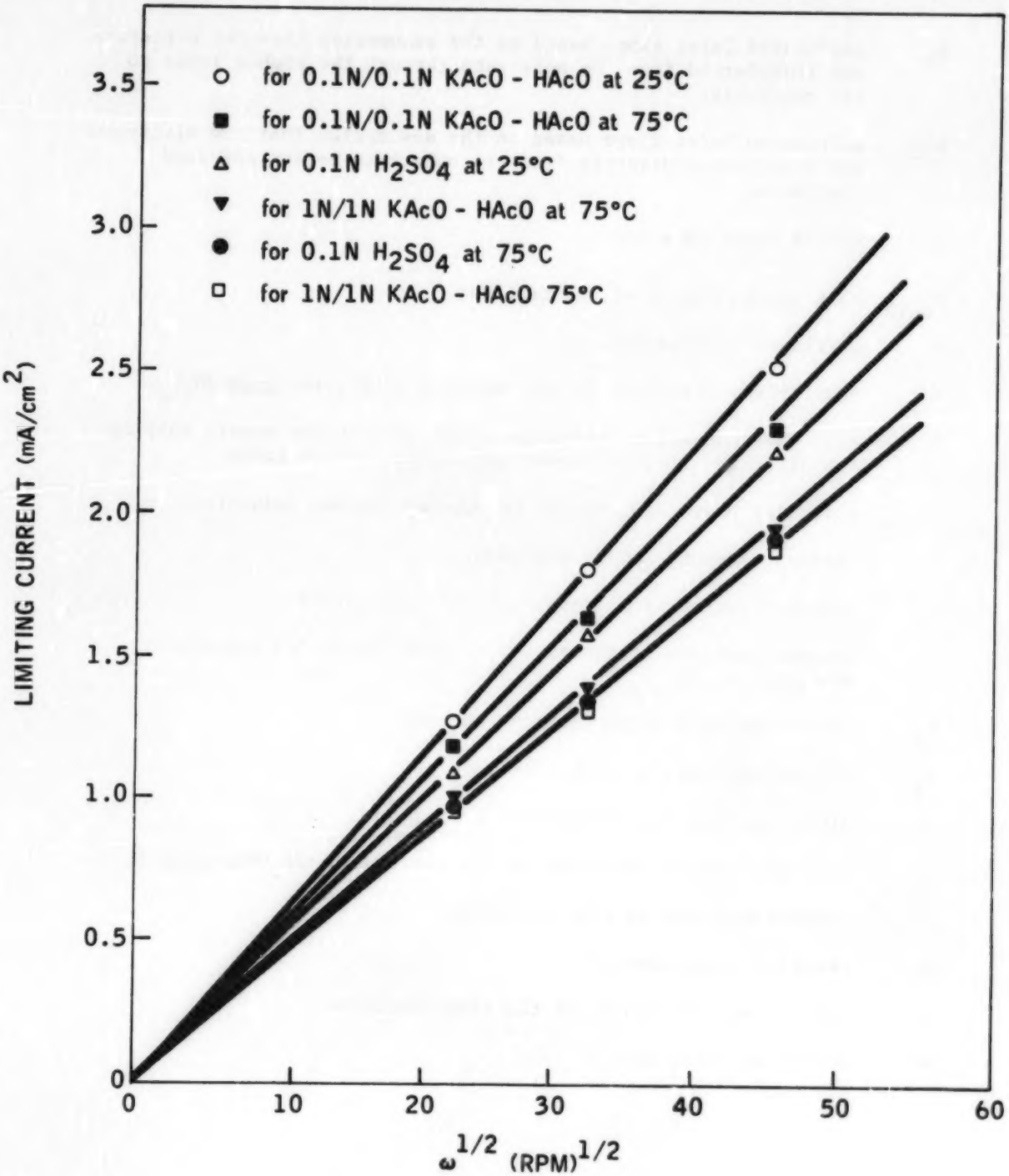

ABBREVIATIONS AND SYMBOLS

b_c calculated Tafel slope based on the assumption that the electrons are transferred from the substrate through the double layer to the reactants.

b'_c calculated Tafel slope based on the assumption that the electrons are transferred directly from the substrate to the adsorbed reactants.

C double layer capacity.

C_{bulk} bulk concentration of the reactant.

D diffusion coefficient.

E equilibrium potential of the reaction $O_2+2H_2O+2e \rightleftharpoons 2H_2O_2$.

$E_{\frac{1}{2}}$ half wave potential, potential where the current equals half of the diffusion limited current of a polarization curve.

$E_{H_2O_2}$, potential where H_2O_2 starts to undergo further reduction.

F Faraday constant, 96500 coulombs.

I measured current for transcient charging curves.

I_o current measured at the potential step occurs for transcient charging curves.

i_a calculated activation limiting current.

i_d current measured on disk electrode.

i_L diffusion limiting current.

i_o exchange current densities of the reaction $O_2+2H_2O+2e \rightleftharpoons 2H_2O_2$.

i_r current measured on ring electrode.

K_i reaction rate constant.

N collecting efficiency for the ring electrode

Re effective resistance

ABBREVIATIONS AND SYMBOLS (cont'd)

RHE	potential with respect to the reversible hydrogen potential in the same solution.
RPM	revolutions per minute
Sc	Schmidt number (ν/D).
SCE	potential with respect to the potential of saturated Caromel electrode.
Z	Abbreviation for $0.62\ D^{2/3}\ \nu^{-1/6}$.
*	surface of the electrode
η	overpotential, the potential difference between the electrode potential and equilibrium potential.
ΔV	potential step applied by the potentiostat.
ω	angular velocity.
ν	kinematic viscosity.

REFERENCES

(1) K. V. Kordesch in "Fuel Cells" Chemical Technology, Vol. 1, I. W. Mitchell, Jr. Ed. Academic Press, New York (1963).

(2) M. R. Tarasevich, F. Z. Sabirov, A. P. Mertsalova and R.K. Burstein, Electrokhimiya 4, 432 (1968).

(3) E. Yeager, P. Krouse and K. V. Rac, Electrochim. Acta 9, 1057 (1964).

(4) I. Morcos and E. Yeager, Electrochim. Acta 15, 953 (1970).

(5) A. J. Appleby and J. Marie, International Society of Electrochemistry, 25th Meeting Brighton - September 22-27, 1974.

(6) EPRI SR-13, Special Report, August 1975.

(7) D. S. Gnanamuthu and J. V. Petrocelli, J. Electrochem. Soc. 114, 1036 (1967).

(8) W. J. Albery and S. Bruckenstein, Trans. Faraday Soc. 62 (7), 1920 (1966).

(9) W. Tiedemann and J. Newman, J. Electrochem. Soc. 122, 70 (1975).

(10) M. Davies, M. Clark, E. Yeager and F. Hovorka, J. Electrochem. Soc. 106, 56 (1959).

(11) R. E. Davis, G. L. Horvath and C. W. Tobias, Electrochim. Acta 12, 287 (1967).